



CHALMERS
UNIVERSITY OF TECHNOLOGY

The role of Pd-Pt Interactions in the Oxidation and Sulfur Resistance of Bimetallic Pd-Pt/ γ -Al₂O₃ Diesel Oxidation Catalysts

Downloaded from: <https://research.chalmers.se>, 2023-05-05 07:12 UTC

Citation for the original published paper (version of record):

Ho, H., Woo, J., Feizie Ilmasani, R. et al (2021). The role of Pd-Pt Interactions in the Oxidation and Sulfur Resistance of Bimetallic

Pd-Pt/ γ -Al₂O₃ Diesel Oxidation Catalysts. Industrial & Engineering Chemistry Research, 60(18): 6596-6612. <http://dx.doi.org/10.1021/acs.iecr.0c05622>

N.B. When citing this work, cite the original published paper.

The role of Pd–Pt Interactions in the Oxidation and Sulfur Resistance of Bimetallic Pd–Pt/ γ -Al₂O₃ Diesel Oxidation Catalysts

Phuoc Hoang Ho, Jung-Won Woo, Rojin Feizie Ilmasani, Joonsoo Han, and Louise Olsson*

Cite This: <https://dx.doi.org/10.1021/acs.iecr.0c05622>

Read Online

ACCESS |



Metrics & More

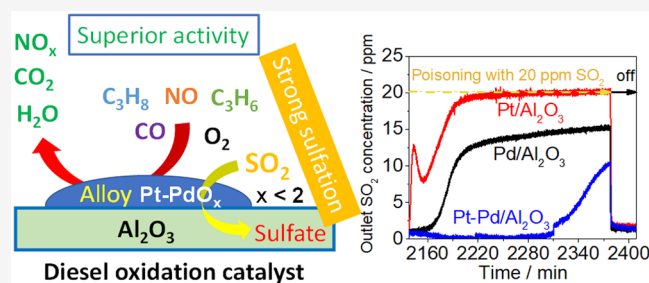


Article Recommendations



Supporting Information

ABSTRACT: Diesel oxidation catalysts (DOC) were investigated for oxidation activity, NO conversion stability, and sulfur poisoning/regeneration on Pd/Al₂O₃, Pt/Al₂O₃, and Pd–Pt/Al₂O₃ catalysts. The Pd/Al₂O₃ catalyst was more active for CO and hydrocarbon (C₃H₆ and C₃H₈) oxidation, while the Pt/Al₂O₃ catalyst efficiently oxidized NO. The formation of a Pd–Pt alloy in the Pd–Pt/Al₂O₃ catalyst maintained Pd in a more reduced phase, resulting in the superior activity of this catalyst for the oxidation of CO, C₃H₆, and NO in comparison with its monometallic counterparts. The Pd–Pt alloy not only provided more low-temperature activity but also retained the stability of NO oxidation. The Pd–Pt alloy also favored the spillover of SO₂ to the alumina support, resulting in significantly higher adsorption capacity of the Pd–Pt/Al₂O₃ catalyst, extensively prolonging its lifetime. However, the stable sulfates on Pd–Pt/Al₂O₃ made it difficult to completely regenerate the catalyst. The bimetallic sample showed higher activity for CO, C₃H₆, and C₃H₈ after sulfur poisoning and regeneration.



1. INTRODUCTION

The diesel oxidation catalyst (DOC) is a key unit in the exhaust after-treatment system (EATS) of diesel engines. The DOC primarily oxidizes CO, unburned hydrocarbons (HCs), and NO and thereby plays an important role in meeting emission regulations.¹ The efficiency of the DOC unit is usually evaluated by the conversion of CO into CO₂, HCs into CO₂ and H₂O, and NO into NO₂. Although NO₂ still must be removed, an optimum level of NO₂ (i.e., NO/NO₂ = 1) would enhance the functions of other downstream units such as regeneration of the diesel particulate filter (DPF) and selective catalytic reduction of NO_x (SCR-deNO_x).^{2,3} Several types of catalysts have been investigated considering both catalyst support and active phase.¹ Pt-based catalysts, especially bimetallic Pt–Pd, are often used in DOC units.¹ The addition of Pd into Pt could improve both the durability of a catalyst against sintering and the catalytic performance of CO and hydrocarbon oxidation.^{4–7} Bimetallic Pt–Pd catalysts are prepared by an impregnation method with different synthesis routes. The most common route is coimpregnation.^{6,8,9} However, a sequential impregnation of Pt/Pd (first Pt and then Pd) or Pd/Pt (first Pd and then Pt) is also used from the literature.^{10–14} The formation of Pt–Pd alloy mainly depends on the temperature and atmosphere of the thermal aging process. In an early study, Morlang et al. have reported that the Pt–Pd alloy was formed even after calcination at 300 °C, or after subsequently reduction in H₂ (500 °C) or thermal aging in the presence of O₂ and water vapor (750 °C).⁶ However, other works have stated that a higher temperature

(e.g., above 500 °C) is required to induce the formation of the Pt–Pd alloy.^{9,15} The formation of Pt–Pd alloy results in a full reduction of the Pt and the partially oxidized and partially metallic character of the Pd in the bimetallic catalysts; however, the distribution of PdO oxide phase is still not clear, it could be adhered at the surface of the alloy particles and/or isolated/dispersed on the alumina support.^{6,9,10}

Diesel fuels always contain a certain level of sulfur, which is converted into SO₂ during the combustion of fuels. The presence of SO₂, even at low levels, is a well-known poison for the DOC.^{8,16} Therefore, understanding the impact of sulfur poisoning is a key factor to retain the lifetime of the DOC. Once SO₂ is present in the feed stream, it could interact with either the support or the active sites of the DOC, and these processes depend on the nature of the active phase, the types of supports, the sulfur concentration, the operation temperature, and other compounds such as water and oxygen.^{17–21} Alumina support is known as a sulfur trap in which sulfur is adsorbed as sulfates, and this process significantly depends on the sulfur source, for example, the process is faster for SO₃ or H₂SO₄ than for SO₂.²² Several studies have been performed to

Special Issue: Enrico Tronconi Festschrift**Received:** November 15, 2020**Revised:** January 31, 2021**Accepted:** February 1, 2021

investigate the deactivation mechanism and impact of SO₂ on the reactivity of Pt/Al₂O₃ catalyst for CO,²³ NO,^{18,24,25} and hydrocarbon oxidation.²⁶ Additionally, many studies have focused on the deactivation of Pd/Al₂O₃ and Pd–Pt/Al₂O₃ catalysts by SO₂ in the complete oxidation of methane.^{19,27–30}

Gracia et al. have reported that in the presence of continuous cofeeding of 20 ppm of SO₂ in 1% CO–10% O₂/He, a higher sulfur storage capacity of alumina than silica was found, which postponed the poisoning of the Pt surface. This subsequently delayed the deactivation of the Pt/Al₂O₃ catalyst compared to that of Pt/SiO₂.²³ However, both catalysts showed the same light-off temperature after extended time-on-stream once the alumina surface had been saturated by SO₂. Those authors have suggested that the presence of SO₂ not only blocked the sites for preferential adsorption of oxygen but also altered Pt–CO bonding.

Li and co-workers have found that the regeneration ability of the Pt/Al₂O₃ catalyst poisoned with SO₂ depended on the exposure time, for example, there was only partial regeneration after 20 h of SO₂ exposure but a complete recovery after a shorter exposure time (5 h).²⁴ The authors have correlated the reversible deactivation with a poisoning of terrace metallic Pt sites, and they have correlated the irreversible deactivation with the poisoning of edge and stepped Pt atoms. When investigating the deactivation of SO₂ on three commercial DOCs and a Pt/Al₂O₃ model catalyst, Kröcher et al. have reported that under a low concentration of SO₂, for example 1 ppm at 250 °C, the catalysts stored a large part of the SO₂ via two processes, comprising fast saturation of the catalyst by sulfuric acid and long-lasting sulfation of the washcoat.¹⁸ The former hampered NO conversion and could be removed between 350 and 400 °C, while the latter formed a more stable compound, for example, aluminum sulfate, which decomposed at higher temperatures. However, when prolonging the time-on-stream up to 22 h on Pt/Al₂O₃, Olsson and Karlsson found that the inclusion of 30 ppm of SO₂ (in a gas mixture containing 630 ppm of NO and 8% O₂ in Ar) caused a significant decrease in NO conversion during the first 30 min, but the NO conversion started to gradually increase after 3 h of time-on-stream from 4.8% to 22.2% at the end of the test.²⁵ This beneficial effect of SO₂ on Pt/Al₂O₃ at 250 °C is linked to the formation of large Pt particles during SO₂ exposure, which is more active for NO oxidation.

In a very early study of hydrocarbon oxidation, Yao et al. found that surface sulfates on Pt/Al₂O₃ promoted the dissociative adsorption of C₃H₈ on Pt and subsequently resulted in significant improvement in the combustion of C₃H₈.³¹ The same trend was reported in other studies.^{32–34} In contrast, the presence of SO₂ has been found to cause a decrease in the conversion for the oxidation of C₃H₆ under reaction conditions similar to those for C₃H₈.^{31,34} The inhibiting impact of SO₂ on the conversion of C₃H₆ depends on the temperature, for example, SO₂ blocks the Pt-active sites below the light-off temperature (<200 °C). However, SO₂ and SO₂-derived species can desorb or diffuse to the bulk alumina above 200 °C, which does not inhibit the Pt-active sites, and as a result, the conversion of C₃H₆ is independent of the presence of SO₂ at higher temperatures.³⁴ Other studies have confirmed the poisoning effect of sulfur for C₃H₆ oxidation on Pt/Al₂O₃ catalysts.^{35,36} However, a positive impact of SO₂ on C₃H₆ oxidation has been reported. The T₅₀ for C₃H₆ oxidation on Pt/Al₂O₃ was found to decrease by almost 30 °C after the

catalyst had been aged with 30 ppm of SO₂ at 800 °C for 2 h followed by sulfur regeneration.³⁷

In summary, the impact of sulfur on the oxidation activity of Pt/Al₂O₃ has been extensively studied for each single model component in diesel exhaust gas emission, for example, CO, NO, C₃H₆, and C₃H₈. In general, the presence of sulfur strongly inhibits the oxidation of CO but promotes C₃H₈ oxidation, while the impact of sulfur is more complex for NO and C₃H₆ oxidation. Although some extended studies have investigated the interaction of sulfur with both monometallic and bimetallic Pd–Pt/Al₂O₃, most of those studies have focused on the impact of sulfur on the oxidation activity of the individual gas, such as CO, NO, C₃H₆, C₃H₈, as aforementioned, and especially CH₄,^{13,19,27,28} or a mixture of gases, such as CO and C₃H₆.³⁸ The performance of the DOC units significantly depends on gas composition.⁸ Consequently, it is necessary to investigate the impact of SO₂ on the DOCs in the presence of a gas mixture, especially with water, which could affect the pathway of sulfur poisoning.³⁰ The objective of this work was to examine the impact of sulfur poisoning and the regeneration of monometallic and bimetallic Pd–Pt/Al₂O₃ catalysts during the simultaneous oxidation of CO, NO, C₃H₆, and C₃H₈ in the presence of H₂O. A series of sequential tests were performed to compare monometallic and bimetallic catalysts in terms of (i) activity and stability during temperature ramps, (ii) the stability of NO conversion, (iii) the effect of reductive treatment, (iv) SO₂ adsorption capacity in correlation with activity at 200 °C during sulfur poisoning, and (v) regeneration under lean/rich conditions of the feed stream and in H₂. The catalysts were thoroughly characterized with inductively coupled plasma sector field mass spectrometry (ICP–SFMS), X-ray diffraction (XRD), transmission electron microscopy (TEM), nitrogen physisorption, CO chemisorption, X-ray photoelectron spectroscopy (XPS), and diffuse reflectance infrared Fourier transform spectroscopy (DRIFTS).

2. EXPERIMENTAL METHODS

2.1. Chemicals. Alumina (γ-Al₂O₃, Sasol, Puralox, SBa-200, specific surface area 190 m² g^{−1}) was used as a support while solutions of Pt(NO₃)₄ (Pt 15% w/w, Alfa Aesar) and Pd(NO₃)₂ (Pd 10% w/w, Alfa Aesar) were used as noble metal precursors. Boehmite (dispersal P2, Sasol), absolute ethanol (Merck), and Milli-Q water were used to prepare a slurry for washcoating.

2.2. Catalyst Preparation. The alumina support was first calcined at 550 °C for 6 h. The support was impregnated with a precursor solution of Pt or Pd to prepare monometallic samples, Pt/Al₂O₃ or Pd/Al₂O₃, respectively. The impregnated material was dried at 90 °C for 16 h, and then calcined in a static oven at 550 °C for 2 h. A bimetallic sample denoted Pd–Pt/Al₂O₃ was also prepared with a two-step impregnation of Pd first and then Pt, and the catalyst was calcined after each impregnation step. Note that the loadings of the noble metals were selected to obtain equimolar amounts of Pt and Pd for comparison.

The powder material was then washcoated on a cordierite honeycomb monolith (400 cpsi (cell per square inch), Ø = 21 mm, L = 20 mm). Prior to washcoating, all bare monoliths were calcined at 600 °C for 2 h. The clean monolith was dipped into a slurry containing approximately 15 wt % of a solid (a mixture of catalyst and binder with a weight ratio of catalyst/binder = 95/5. Boehmite from Sasol, Dispersal P2, was used as the binder) and 85 wt % liquid (water/ethanol =

50/50 weight ratio). The monolith was calcined at 550 °C at a ramping rate of 5 °C min⁻¹ for 2 h after washcoating. The targeted total mass of washcoat on each monolith was approximately 500 ± 10 mg.

2.3. Catalyst Characterization. Note that all characterizations (except ICP-SFMS) were performed on the samples that were degreened and pretreated (see section 2.4.1) to investigate the properties of the catalysts before the reaction.

2.3.1. Inductively Coupled Plasma Sector Field Mass Spectrometry (ICP–SFMS). Pt and Pd loadings in the calcined catalysts were determined with ICP–SFMS analysis performed by ALS Scandinavia (Luleå, Sweden).

2.3.2. X-ray Diffraction (XRD). XRD measurements were carried out using a D8 Advance Diffractometer (Bruker AXS, Germany, Cu K α radiation). Wide-angle diffractograms were collected over 2 θ range from 20 to 90° with a step size of 0.02° and scan time of 1 s per step. The average crystallite sizes of Pt⁰ and PdO denoted d_c , were determined using the Scherrer eq (eq 1) in which the full width at half-maximum (β) of the Pt(111) and PdO(112) plane was corrected with the Warren equation (eq 2) with alumina as the reference. The Bragg angles θ at Pt(111) and PdO(112) reflection were determined from the XRD pattern. The wavelength λ of the Cu K α and the shape factor K_F were 0.15406 nm and 0.89, respectively.³⁹

$$d_c = \frac{K_F \lambda}{\beta \cos \theta} \quad (1)$$

$$\beta = \sqrt{\beta_{\text{observed}}^2 - \beta_{\text{reference}}^2} \quad (2)$$

2.3.3. Nitrogen Physisorption. Nitrogen physisorption measurements were performed at –196 °C using a Micromeritics Tristar instrument. About 0.15 g of powder catalyst was degassed at 250 °C for 8 h. The specific surface area (S_{BET}) was calculated using the Brunauer–Emmett–Teller (BET) multiple-point method in the relative pressure range p/p_0 from 0.05 to 0.3.

2.3.4. CO Chemisorption. Metal dispersion was determined with CO chemisorption using an ASAP2020 Plus instrument (Micromeritics). About 0.1 g of powder catalyst was degassed in He, evacuated in vacuum at 110 °C, and reduced in H₂ at 400 °C for 1 h. The sample was then evacuated to 5 μ mHg at 400 °C for 30 min before being cooled to 35 °C. The sample was further evacuated to 5 μ mHg at 35 °C, and a leak test was performed. After that, it was evacuated to 5 μ mHg before the first isotherm (total isotherm) was performed in the pressure range from 100 to 600 mmHg (interval of 25 mmHg). When the first isotherm was completed, the sample was evacuated to remove physically adsorbed CO before the second isotherm was repeated. The difference between the two isotherms provided the isotherm of chemisorbed CO. The intercept of a linear regression curve fit from the isotherm of chemisorbed CO was attributed to the amount of adsorbed CO on a monolayer of the metal surface. The dispersion was calculated with eq 3:

$$D_M(\%) = \frac{F_s N_{\text{CO}}}{N_M} 100 \quad (3)$$

where N_M is the total number of atoms of metal, N_{CO} is the number of CO molecules adsorbed on the monolayer, and F_s is a stoichiometric factor considering the form of CO adsorption on the metal. The stoichiometry factor was 1 and 2 for Pt- and

Pd-based catalysts, respectively.^{40,41} The crystallite size was reported based on the assumption of hemispheric particles.

2.3.5. Transmission Electron Microscopy (TEM). TEM characterization was carried out with an FEI Titan 80–300 microscope equipped with a Cs-corrector probe and a high-angle annular dark-field (HAADF) detector and energy dispersive spectroscopy (EDS). Fine catalyst powder (the degreened sample) was dispersed into absolute ethanol and sonicated for 15 min. One drop of the obtained suspension was distributed onto carbon-coated Cu grids. Average particle size and size distribution were determined by counting >150 particles using ImageJ software.

2.3.6. X-ray Photon Spectroscopy (XPS). X-ray photoelectron spectroscopy (XPS) analyses were performed using a PerkinElmer PHI 5000 VersaProbe III scanning XPS microprobe apparatus. The X-ray source was generated from monochromatic Al K α radiation (energy 1486.6 eV), and the beam size diameter was 100 μ m. The system was aligned with Au (83.96 eV), Ag (368.21 eV), and Cu (932.62 eV), and the binding energy was calibrated with the carbon peak C1s at 284.8 eV before performing narrow scan measurements. It should be noted that Pt4f5/2 and Al2p lines overlapped. To distinguish Pt4f5/2 and Al2p, Pt4f7/2 was determined first since its binding energy was visible, and then an energy separation of 3.33 eV and a 4:3 intensity ratio between Pt4f5/2 and Pt4f7/2 was routinely used as constraints in the line fitting to deconvolute separately the photoelectron line of Pt4f5/2 from its overlapping with Al2p.

2.3.7. Diffuse Reflectance Infrared Fourier Transform Spectroscopy (DRIFTS). In situ DRIFTS spectra were recorded on a Vertex 70 spectrometer equipped with a liquid nitrogen cooled MCT (mercury cadmium telluride) detector. Sample powder was placed in a high-temperature reaction cell (Harrick Praying Mantis) equipped with a CaF₂ window. A thermocouple was installed in the middle of the cell to monitor the temperature of the sample. The temperature was regulated with a Eurotherm 2416 controller, while the gas flows were controlled with mass flow controllers (Bronkhorst Hi-Tech). Prior to the experiment, each catalyst was pretreated at 500 °C with 10 vol % O₂/Ar for 15 min and then cooled to 35 °C. The background was recorded at this temperature, and thereafter a flow of 0.1 vol % CO/Ar was introduced to the cell. The spectra were recorded every minute for 30 min when the sample was exposed with CO. After that the CO flow was switched off, and the sample was purged with Ar for 10 min before the last spectrum was recorded.

2.4. Catalytic Tests. The oxidation performance of the catalysts was tested using a flow reactor system consisting of a horizontal quartz tube (i.d. 21 mm \times L 780 mm), a heating system (Eurotherm temperature controller), eight mass flow controllers (MFC, Bronkhorst), a controlled evaporator and mixer (CEM) to supply water vapor (Bronkhorst), and an online-gas analyzer (MultiGasTM 2030 FTIR, MKS). Two K-type thermocouples, one in front (distance about 2 cm) and one in the middle of the monolith, were used to measure the temperature of the inlet gas stream and inside the monolith, respectively.

2.4.1. Degreening and Pretreatment. Degreening and pretreatment steps are necessary to activate the catalyst to a well-defined and stable state before performing the catalytic tests. For degreening, the monolith was first reduced in a gaseous mixture containing 2 vol % H₂ and 5 vol % H₂O/Ar at 500 °C for 30 min and then oxidized in a mixture of 500 ppm

of NO, 8 vol % O₂, and H₂O/Ar at 700 °C for 2 h. The catalyst was then cooled to 500 °C and subjected to a pretreatment procedure. The pretreatment was performed at 500 °C in five sequential steps (15 min for each) in different gas mixtures, namely, 10 vol % O₂ and 5 vol % H₂O/Ar; 5 vol % H₂O/Ar; 1 vol % H₂ and 5 vol % H₂O/Ar; 5 vol % H₂O/Ar; and 10 vol % O₂ and 5 vol % H₂O/Ar. Eventually, the catalyst was cooled to 120 or 150 °C depending on the subsequent experiment.

For catalyst characterization, the degreening was performed with catalyst powder placed in a crucible in the reactor. The catalyst powder was exposed to the same conditions for degreening as the monolith.

2.4.2. Activity Tests. Each catalyst was tested in a sequential experiment, as shown in Figure 1. The sequences were as

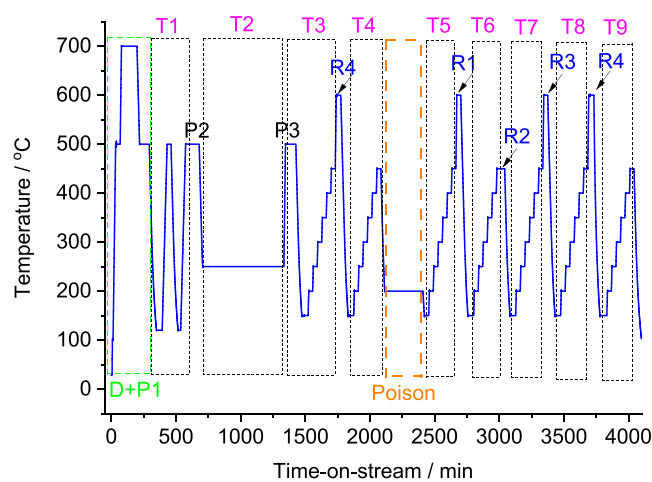


Figure 1. Description of experiments used to examine the DOCs in a flow reactor. D+P1 stands for degreening and pretreatment (see section 2.4.1). Test T1: two cycles of ramping mode from 120 to 500 °C (10 °C min⁻¹); pretreatment P2. T2: stability test of NO oxidation for 10 h at 250 °C (Pt-based catalysts), or a total of 10 h at 250, 300, 350, 400, 450 °C (2 h at each temperature for the Pd-only catalyst); pretreatment P3. T3: test at seven points of temperature 150–450 °C (interval 50 °C, 30 min for each step). Regeneration R4: reduction in H₂ at 600 °C for 30 min. T4 test (same as T3); sulfur poisoning at 200 °C in gas mixture + 20 ppm of SO₂. T5 test (same as T3); Regeneration R1; T6 test (same as T3); Regeneration R2; T7 test (same as T3); Regeneration R3; T8 test (same as T3); Regeneration R4; T8 test (same as T3). Detailed information about the gas compositions of each test is given in Table 1.

follows: (i) oxidation with two cycles of ramping the temperature from 120 to 500 °C (denoted T1); (ii) stability test of NO oxidation, 10 h at 250 °C for Pt-based catalysts, and 10 h at 250, 300, 350, 400, 450 °C (2 h for each temperature)

for the Pd-only catalyst (T2); (iii) oxidation with (T4) and without (T3) prerduction of the catalyst; (iv) sulfur poisoning with 4 h in the gas mixture as T1–T4 but with the addition of 20 ppm of SO₂ at 200 °C; and (v) a regeneration and activity test after each regeneration step (T5 to T9, R1 to R4), see section 2.4.3 for a detailed description.

Another sequence of the experiment was performed on the second monolith of Pt/A₂O₃ to investigate the effect of hydrocarbons on the oxidation of NO. After the degreening and pretreatment step (see section 2.4.1), the first experiment was performed in a standard gas mixture containing 500 ppm of NO, 10 vol % O₂, and 5 vol % H₂O balanced in Ar. The temperature was increased from 120 to 500 °C with a ramp of 10 °C min⁻¹. This experiment was repeated, with also adding C₃H₈ into the standard gas mixture with different concentrations, 250, 500, and 1000 ppm, corresponding to a NO/C₃H₈ ratio of 2:1, 1:1, and 1:2, respectively. Finally, 500 ppm of C₃H₆ was added into the mixture with a NO/C₃H₈ ratio of 1:1. Before each test, the catalyst was pretreated (see section 2.4.1).

2.4.3. Regeneration. Four different steps were employed to regenerate the catalyst after a 4 h duration of SO₂ poisoning. The duration of each regeneration step was 30 min. The gas composition used in each regeneration step is given in Table 1. In the first step, R1, the catalyst was heated to 600 °C in the presence of the reactants (lean condition), whereas in the R2 and R3 steps, the catalyst was maintained at 450 and 600 °C, respectively, in rich condition (the O₂ flow was shut-off). In the last step, R4, the catalyst was reduced in H₂ at 600 °C. The tests T5 to T9 were performed after each regeneration step and were compared for catalyst regeneration. SO₂, SO₃, and H₂SO₄ were measured during the regeneration; however, the concentrations of SO₃ and H₂SO₄ were negligible and could therefore not be processed with adequate accuracy. The main SO_x source observed was SO₂, which was used for the discussion in section 3.2.4.

3. RESULTS AND DISCUSSION

3.1. Catalyst Characterization. The Pt and Pd contents obtained with the ICP-SFMS analysis were 1.8 and 1.0 wt % for monometallic Pt/Al₂O₃ and Pd/Al₂O₃, respectively (Table 2). The bimetallic Pd–Pt/Al₂O₃ catalyst contained 1.0 wt % Pt and 0.7 wt % Pd. Note that these loadings resulted in a similar total mole of noble metals in each sample. These low loadings of noble metals did not significantly alter the surface area of the alumina support; the three impregnated samples showed very similar specific surface areas approximately 177–181 m² g⁻¹ (Table 2).

Table 1. Gas Composition for the Catalytic Tests and Regeneration. The Compositions Were Balanced with Ar in All Tests

test	gas/ppm							
	CO	NO	C ₃ H ₆	C ₃ H ₈	O ₂ /vol %	H ₂ O/vol %	H ₂ /vol %	SO ₂
T1	1000	500	500	500	10	5		
T2		500			10	5		
T3–T9	1000	500	500	500	10	5		
sulfur poisoning/4 h	1000	500	500	500	10	5		20
R1/600 °C	1000	500	500	500	10	5		
R2/450 °C	1000	500	500	500		5		
R3/600 °C	1000	500	500	500		5		
R4/600 °C								

Table 2. Physico-Chemical Properties of Monometallic and Bimetallic Pd–Pt/Al₂O₃ Catalysts

catalyst	loading/wt %		$S_{\text{BET}}/\text{m}^2\text{ g}^{-1}$	CO chemisorption			particle size/nm		
	Pd	Pt		CO/ $\mu\text{mol g}^{-1}$	CO/Mmol/mol	dispersion /%	CO chemisorption	STEM	XRD
Pd/Al ₂ O ₃	1.2		181	42.8 \pm 0.4	0.38	76	1.5	12.1	10
Pt/Al ₂ O ₃		1.8	177	17.6 \pm 0.4	0.18	18	6.3	2.0	20
Pd–Pt/Al ₂ O ₃	0.7	1.0	180	14.8 \pm 0.4	0.13	20		7.4	13 ^a

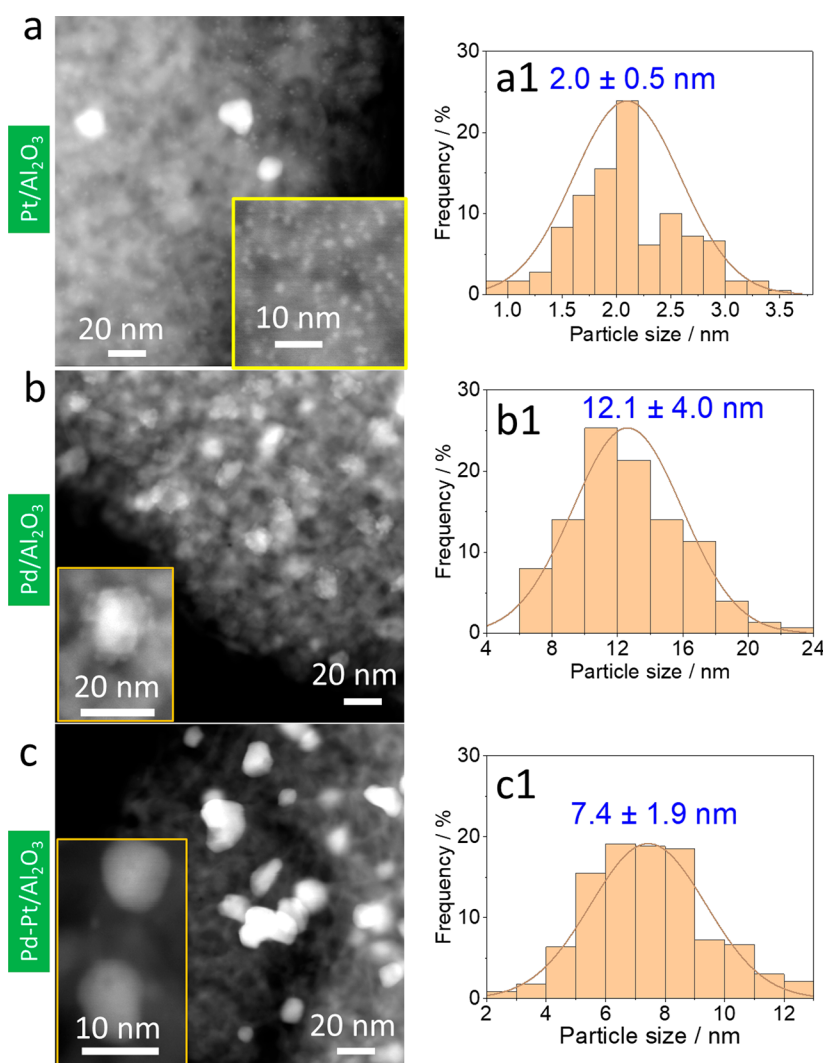
^aFor Pt particle.Figure 2. TEM images and particle size distribution of Pt/Al₂O₃, Pd/Al₂O₃, and Pd–Pt/Al₂O₃ catalysts.

Figure 2 presents TEM images of Pt/Al₂O₃, Pd/Al₂O₃, and Pd–Pt/Al₂O₃ catalysts after the degreening treatment. The alumina support had a needle-like morphology on which the particles of the supported metal were dispersed. Most Pt particles were homogeneously distributed on the alumina surface of Pt/Al₂O₃ with an average particle size distribution of approximately 2.0 nm together with a few large and agglomerated particles (10–20 nm) (Figure 2a, a1). Both small and large particles of Pd/Al₂O₃ were observed. In addition, larger Pd clusters of small particles were found; however, it was difficult to distinguish the individual Pd particles in the agglomerates, and the size of the agglomerates was used instead. This resulted in an overestimation of the particle size of this sample. The average particle/cluster size was approximately 12.1 nm (Figure 2b, b1). The bimetallic

Pd–Pt/Al₂O₃ sample showed both small and large particles in a range of 2–13 nm with an average particle size of approximately 7.4 nm (Figure 2c, c1). Pd–Pt/Al₂O₃ had a smaller particle size distribution than Pd/Al₂O₃, indicating an improvement in the sintering resistance of Pd particles in the presence of Pt at high temperatures, which is in line with the literature.^{8,42} It should be noted, however, that the clusters were also included in the dispersion evaluation of Pd/Al₂O₃, consequently, an exact comparison cannot be made. To analyze the distribution of Pd and Pt in the bimetallic Pd–Pt/Al₂O₃ catalyst, STEM-EDS images were taken. Figure 3 presents the distribution of Pd, Pt, and Al elements. The overlap of the Pd and Pt signals (Figure 3c, d) with the bright spots from the HAADF TEM image (Figure 3a) indicates a uniform elemental composition of the clusters. This result also

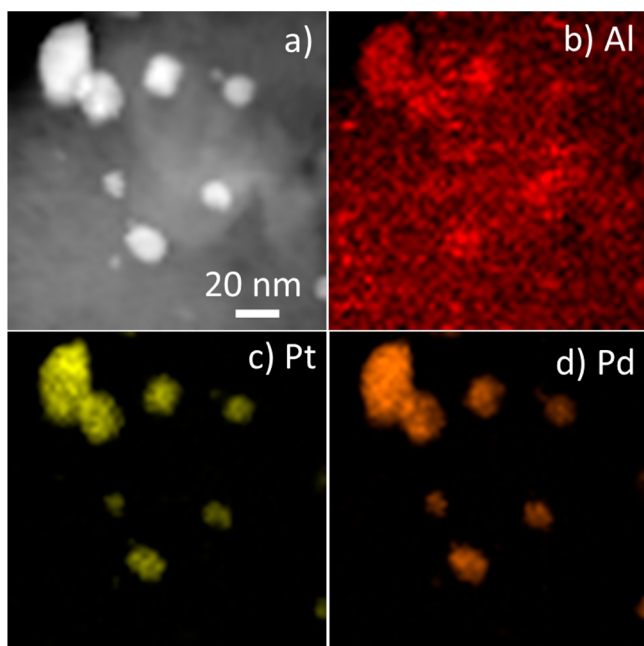


Figure 3. HAADF TEM images and EDS maps for the Pd–Pt/Al₂O₃ catalyst: (a) TEM image, (b) Al-K line, red, (c) Pt-L line, yellow, and (d) Pd-L line, orange. The bar scale in panel a is the same for all panels.

demonstrated that Pt and Pd are interacting and not distributed separately on the support surface. This finding suggests an alloy formation.

The XRD patterns (Figure 4) show broad reflections of the γ -Al₂O₃ support (PDF #01-076-3264). Metallic Pt (PDF #04-

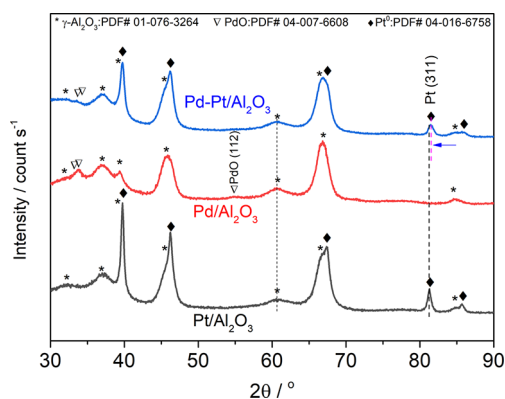


Figure 4. X-ray diffraction patterns of Pt/Al₂O₃, Pd/Al₂O₃, and Pd–Pt/Al₂O₃ catalysts.

016-6758) and PdO (PDF #041-007-6608) were also identified on Pt/Al₂O₃ and Pd/Al₂O₃, respectively, while both Pt and PdO were found on bimetallic Pd–Pt/Al₂O₃, in line with the literature.^{8–10} No other oxide phase of Pt was identified, although Pt/Al₂O₃ and Pd–Pt/Al₂O₃ were degreened at 700 °C in an oxidizing environment. Interestingly, the diffraction angle of Pt(311) in the bimetallic sample ($2\theta = 81.5^\circ$) shifted slightly to a higher angle than the angle of Pt/Al₂O₃ ($2\theta = 81.3^\circ$), while no change in the diffractions of the support occurred. These results suggest the formation of a Pt–Pd alloy, as reported by Graham and co-workers.¹⁵ However, this was not observed in the bimetallic sample after the only calcination at 550 °C (before the degreening)

(Figure S1, Supporting Information), indicating that the Pd–Pt alloy had mainly been formed during the degreening step wherein the sample was treated at 700 °C. Martin and co-workers have reported the formation of a Pt–Pd alloy at 800 °C but not at 500 °C under treatment in air or air in the presence of water,⁹ which supports our findings. The Pt(311) peak of bimetallic Pd–Pt/Al₂O₃ was broader and less intense than the peak of the monometallic Pt/Al₂O₃, suggesting that the sintering of the Pt particles had been suppressed in the bimetallic sample. The mean crystallite sizes of the metallic Pt (reflection (311)) calculated by using the Scherrer equation were found to be 20 and 13 nm for Pt/Al₂O₃ and Pd–Pt/Al₂O₃, respectively. The crystal size of the PdO (reflection (112)) from Pd/Al₂O₃ was approximately 10 nm, whereas it was not possible to calculate the crystal size for PdO from Pd–Pt/Al₂O₃ due to the weak intensity of the reflection (112) on this sample. Note that in the X-ray diffraction, the coherent scattering area of crystalline particles smaller than 2 nm is not large enough to contribute significantly to the Bragg reflections, and consequently, the particle sizes obtained with XRD are often overestimated.⁶ The particle sizes of Pd/Al₂O₃ determined with TEM were mainly based on large clusters, and therefore they were close to the sizes determined with XRD since both analyses considered large particles. A discrepancy in the average particle sizes determined with XRD and TEM was found for Pt/Al₂O₃. This discrepancy was because XRD accounted for large particles, while TEM included small particles.

CO chemisorption measurements were performed to complement the XRD and TEM analyses of particle size, and the data are summarized in Table 2. The amounts of adsorbed CO were 42.8 and 17.6 $\mu\text{mol g}^{-1}$, resulting in dispersions of 76 and 18% for Pd/Al₂O₃ and Pt/Al₂O₃, respectively. Note that the calculated dispersions were based on the stoichiometric factor of CO of 1 and 2 for Pt/CO and Pd/CO, which corresponds to a linear and bridged carbonyl adsorption geometry, respectively. Our DRIFTS data (Figure 6) showed that only linear carbonyl CO adsorbed onto Pt/Al₂O₃ while both linear and bridged CO carbonyl were observed on Pd/Al₂O₃. Although the exact ratio between linear and bridged carbonyl is not known; stoichiometric adsorption of Pd/CO = 2 has been widely used in the literature,^{40,43} and was also adopted in this study, but it should be noted that this could lead to a somewhat underestimation of the Pd dispersion. The larger dispersion of Pd than Pt is equivalent to smaller mean particle size, 1.5 and 6.0 nm, respectively. Bimetallic Pd–Pt/Al₂O₃ showed a dispersion of 20%, which is slightly higher than that of Pt/Al₂O₃. We suggest that the discrepancy in particle sizes of PdO and Pt between HR-TEM and CO chemisorption is because of the differences in the methods. CO chemisorption provides information for the whole samples, while TEM gives information regarding the local positions of the samples. For example, TEM shows an average size of 12.1 nm, whereas CO chemisorption gives an average size of 1.5 nm for Pd/Al₂O₃. This could be because the smallest Pd particles were not observed in our TEM images, and besides that we could not resolve the Pd sizes in the Pd clusters. In contrast, for CO chemisorption measurements, CO can access the whole sample, and CO chemisorption thereby provides more precise information on the average size of Pd in the sample. Such discrepancy of the average sizes determined by TEM and chemisorption has also been reported in the literature earlier.⁴⁴

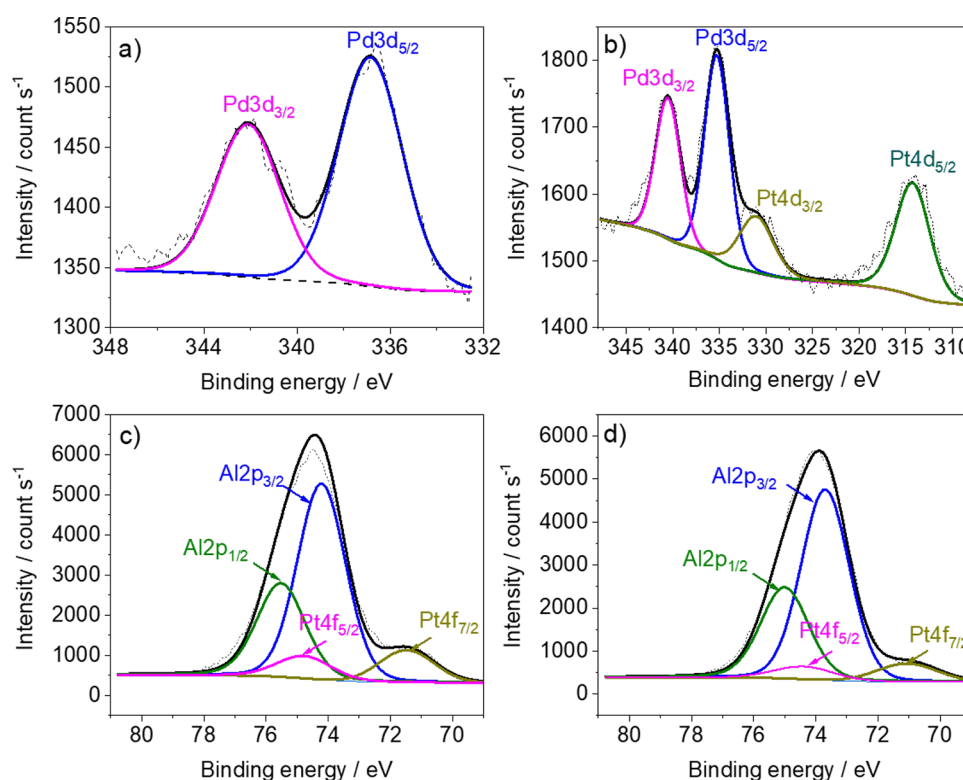


Figure 5. X-ray photoelectron spectra of Pd/Al₂O₃, Pt/Al₂O₃, and Pd–Pt/Al₂O₃ catalysts: (a) Pd3d of Pd/Al₂O₃, (b) Pd3d of Pd–Pt/Al₂O₃, (c) Pt4f of Pt/Al₂O₃, and (d) Pt4f of Pd–Pt/Al₂O₃. The dotted and solid black lines are the original and fitting curves, respectively, of the spectra.

XPS measurements were performed to examine the surface oxidation states of the noble metal phases. The spectra recorded for the core levels of Pd3d, Pt4f, and Al2p are presented in Figure 5, while the binding energy (B.E.) values are summarized in Table 3. Pd/Al₂O₃ showed a B.E. of Pd3d5/

Table 3. Binding Energy of Pd3d5/2, Pt4f7/2, and O1s Identified from XPS of Pd/Al₂O₃, Pt/Al₂O₃, and Pd–Pt/Al₂O₃ Catalysts

core	binding energy/eV		
	Pd/Al ₂ O ₃	Pd–Pt/Al ₂ O ₃	Pt/Al ₂ O ₃
Pd 3d5/2	336.9	335.3	
Pt 4f7/2		71.1	71.5

2 core at 336.9 eV, suggesting the presence of a Pd²⁺ oxidation state. While Pt/Al₂O₃ had a Pt4f7/2 core level of approximately 71.5 eV, which was close to the standard value of metallic Pt (approximately 71 eV), suggesting an abundant amount of metallic Pt on the surface of this catalyst, but also likely small amounts of oxides.⁴⁵ Interestingly, the bimetallic Pd–Pt/Al₂O₃ sample exhibited Pd3d5/2 and Pt4f7/2 core levels at 335.3 and 71.1 eV, respectively, suggesting that both Pd and Pt were in metallic form on the surface of this sample. Note that the ultrahigh vacuum treatment during sample preparation before measurements could lead to a partial reduction of PdO.⁴⁶ However, the most important conclusion is that Pt was fully reduced in the bimetallic Pd–Pt/Al₂O₃ sample after degreening, and Pd existed in a more reduced form (lower oxidation state) than its monometallic counterparts. We suggest that this is related to the formation of a Pd–Pt alloy; alloy formation is also supported by the XRD results (Figure 4) and TEM-EDS (Figure 3). Our results are in

line with the study by Johns and co-workers, who found that Pt had been fully reduced, and almost 70% of the Pd species were in the metallic phase when the authors examined the microstructure of bimetallic Pt–Pd catalysts aged in the air at 750 °C.¹⁰

Figure 6 presents the DRIFTS measurements of CO adsorption onto Pd/Al₂O₃, Pt/Al₂O₃, and Pd–Pt/Al₂O₃. As shown in Figure 6a, Pd/Al₂O₃ had two main broad peaks at approximately 2098 and 1938 cm^{−1} after 30 min of CO exposure in a flow of 100 mL min^{−1} of 1000 ppm of CO in Ar at atmospheric pressure. The main peak at 2098 cm^{−1} and a shoulder at 2060 cm^{−1} were assigned to linear CO adsorption onto metallic Pd (Pd⁰–CO) with different particle sizes.^{47,48} The shoulders at the higher wavenumber 2135 and 2123 cm^{−1} were assigned to CO adsorbed onto cationic Pd²⁺–CO and Pd⁺–CO.⁴⁹ Note that the band 2135 cm^{−1} is quite close to the value of 2138 cm^{−1} for physically adsorbed CO (which was usually observed under high pressure of CO).⁵⁰ Moreover, this band was only observed on Pd/Al₂O₃ and Pd–Pt/Al₂O₃ but not on the Pt/Al₂O₃ catalyst (Figure 6a). In addition, the band was not removed (only decreased) during Ar flushing after the CO exposure. These results, therefore, suggest that the band at 2135 cm^{−1} is not associated with physically adsorbed CO. The band at 1938 cm^{−1} has been reported to be associated with bridging CO adsorption onto either Pd⁺ or metallic Pd species.^{28,51–53} However, the presence of this band even in the first spectrum directly after the catalyst was exposed to CO flow (Figure 6b), combined with the absence of a metallic Pd in the degreened catalyst (as identified with both XRD and XPS), suggest that the band at 1938 cm^{−1} is related to bridging CO on Pd⁺. The spectra for CO adsorption onto Pd/Al₂O₃ in Figure 6b show that the main IR bands when starting the CO adsorption are associated with Pd²⁺–CO, which is in line with

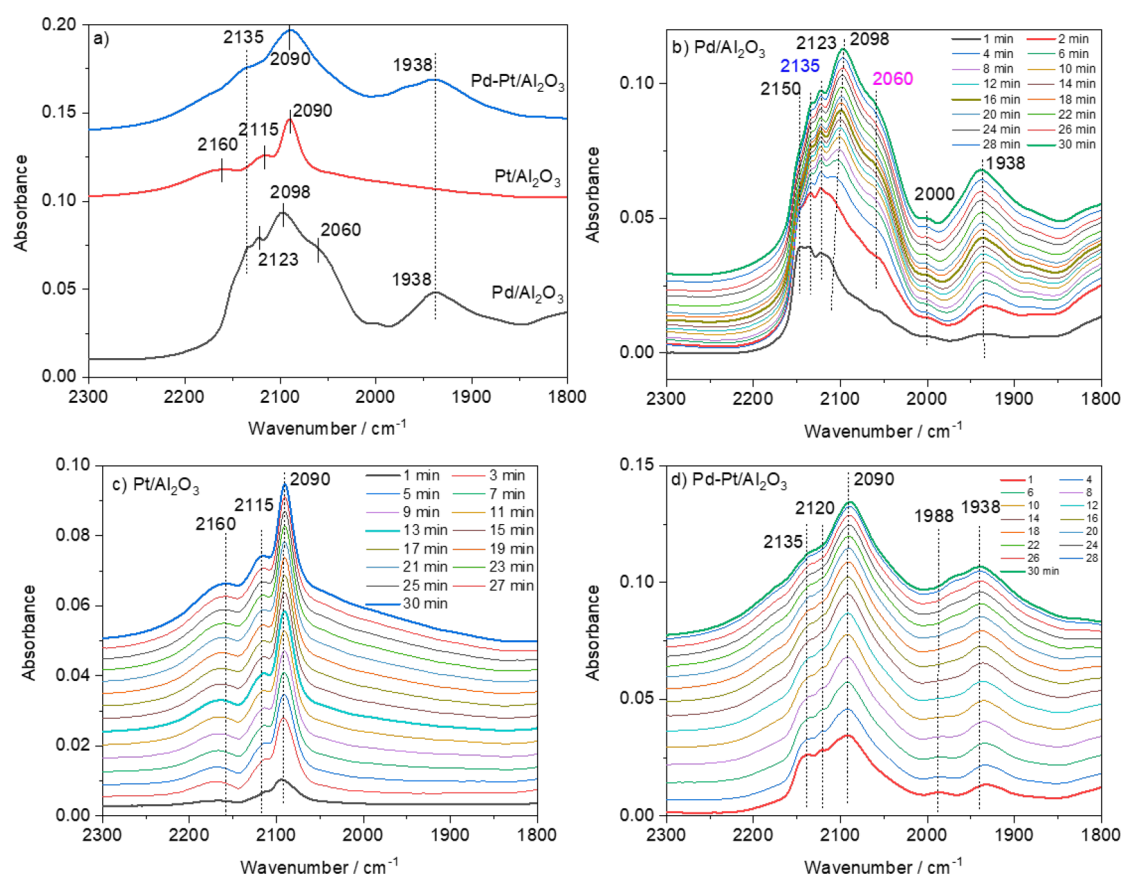


Figure 6. CO DRIFTS spectra performed on Pd/Al₂O₃, Pt/Al₂O₃, and Pd–Pt/Al₂O₃: (a) comparison of the last spectrum of each sample (purging with 100 mL min^{−1} of Ar for 10 min after stopping CO gas); and (b–d) spectra with time-on-stream during CO adsorption in a flow of 100 mL min^{−1} of 1000 ppm of CO with Ar balance gas at atmospheric pressure. The samples were treated in 10 vol% O₂/Ar at 500 °C for 30 min and then cooled to 35 °C in Ar before CO adsorption measurements.

XPS and XRD data. When the time for CO exposure is increased the Pd²⁺–CO increased slowly in intensity, whereas the bands of Pd⁺–CO and Pd⁰–CO were more intense and rapidly increased with the time-on-stream of CO exposure. This indicates that the Pd²⁺ was partially reduced to Pd⁺ and metallic Pd during CO adsorption.

In contrast, the main IR bands for Pt/Al₂O₃ were observed at 2090, 2115, and 2160 cm^{−1} (Figure 6a), and the entire spectrum exhibited a uniform shape without any significant shift in peak positions during the 30 min of CO adsorption (Figure 6c). The most intense peak at 2090 cm^{−1} was assigned to CO linearly adsorbed onto metallic Pt,^{54,55} whereas the second (2115 cm^{−1}) and the third peaks (2160 cm^{−1}) corresponded to CO adsorbed onto monatomic metallic Pt species, and CO weakly coordinated to Pt ions, respectively.^{56,57}

Adsorption of CO for 30 min onto bimetallic Pd–Pt/Al₂O₃ resulted in three main IR bands at 2135, 2090, and 1938 cm^{−1} (Figure 6a). The band at 2090 cm^{−1} was ascribed to CO linearly adsorbed onto metallic Pt while the bands at 2135 and 1938 cm^{−1} were assigned to CO adsorption onto Pd²⁺ and Pd⁺, respectively, similar to the monometallic samples. Additionally, a weak band at approximately 1988 cm^{−1} (Figure 6d) appeared in the spectrum of Pd–Pt/Al₂O₃ suggesting the presence of metallic Pd in this sample.⁵² Finally, the bands at 2135 (Pd²⁺–CO) and 2120 cm^{−1} (Pd⁺–CO) almost retained their relative intensities to the band at 2090 cm^{−1}, unlike those observed on

Pd/Al₂O₃. This suggests that Pd cations are more stable in Pd–Pt/Al₂O₃ than Pd/Al₂O₃ during CO adsorption.

In summary, all characterization results indicate that the nature of Pd and Pt species are different for monometallic and bimetallic Pd–Pt catalysts. PdO is the main phase in Pd/Al₂O₃, whereas metallic Pt is the major component in Pt/Al₂O₃. The results suggest that the bimetallic Pd–Pt/Al₂O₃ catalyst contains Pd–Pt alloy, in which the metallic Pt maintained the Pd in a more reduced form (lower oxidation state than Pd²⁺) unlike Pd/Al₂O₃, in which Pd was fully oxidized in the form of PdO. In line with the literature, we found that the presence of Pt in the Pd–Pt bimetallic catalyst provided some beneficial effects such as the weakened bond strength of Pd–O and an increase in the Pd/PdO ratio.^{11,14,58}

3.2. Activity Test. After being degreased and pretreated to activate and stabilize the active sites, the catalysts were tested in a sequential experiment as described in Figure 1. The focus of this section will be on comparisons of the three catalysts in terms of baseline catalytic activity, NO conversion stability, sulfur resistance, and sulfur regeneration.

3.2.1. Baseline Catalytic Activity. The catalytic tests were performed in the simulated exhaust gas. Figure 7 presents the light-off curves for CO, NO, C₃H₈, and C₃H₆ obtained for Pd/Al₂O₃, Pt/Al₂O₃, and Pd–Pt/Al₂O₃ catalysts. Table 4 summarizes the temperatures at which 50% (*T*₅₀) or 90% (*T*₉₀) of each gas was converted and Figure S2 shows the NO₂ and N₂O concentrations. Two ramp-cycle tests were sequentially performed on each catalyst without pretreatment

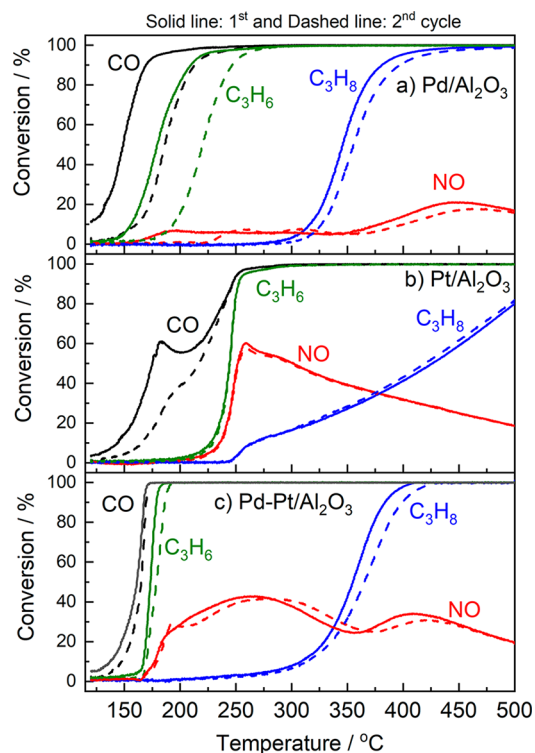


Figure 7. Conversion of CO, C₃H₆, NO, and C₃H₈ on (a) Pd/Al₂O₃, (b) Pt/Al₂O₃, and (c) Pd–Pt/Al₂O₃ catalysts; total flow rate of 2600 mL min^{−1} (standard temperature and pressure STP) containing 1000 ppm of CO, 500 ppm of NO, 500 ppm of C₃H₆, 500 ppm of C₃H₈, 10 vol % O₂, and 5 vol % H₂O balanced in Ar. GHSV = 22 520 h^{−1}.

Table 4. T_{50} and T_{90} Values of CO, C₃H₆, NO, and C₃H₈ on Monometallic and Bimetallic Pd–Pt/Al₂O₃

gas	cycle	Pd/Al ₂ O ₃		Pt/Al ₂ O ₃		Pd–Pt/Al ₂ O ₃	
		T_{50}	T_{90}	T_{50}	T_{90}	T_{50}	T_{90}
CO	1st	149	169	175	247	160	166
	2nd	186	213	217	247	164	168
NO	1st			252			
	2nd			253			
C ₃ H ₈	1st	346	381	426		353	382
	2nd	356	397	419		364	398
C ₃ H ₆	1st	180	210	244	252	172	177
	2nd	220	247	245	252	177	185

in between. The results in Figure 7 clearly show that the light-off curves of all the components for Pd/Al₂O₃ shifted to higher temperatures in the second cycle (dashed lines) than those in the first cycle (solid lines), and the shifts were more pronounced for CO and C₃H₆ than for C₃H₈ and NO. In contrast, the light-off curves for Pt/Al₂O₃ were almost identical between the two cycles, except for CO for which the low-temperature range of the second cycle shifted. The bimetallic Pd–Pt/Al₂O₃ catalyst showed minor shifts in the light-off curves in the second cycle for all components. These observations suggest that the Pt/Al₂O₃ catalyst exhibited greater stability than the Pd/Al₂O₃ catalyst, likely because it had more resistance to noble metal oxidation. Interestingly, the bimetallic catalyst also had the same good oxidation resistance as monometallic Pt/Al₂O₃.

We used the light-off curves of the second cycle to compare activity among the catalysts. The oxidation activity of both Pd/

Al₂O₃ and Pt/Al₂O₃ followed a similar trend, that is, CO < C₃H₆ < NO < C₃H₈, although the activity for each component was different. The Pd/Al₂O₃ catalyst had significantly lower T_{50} values for CO, C₃H₆, and C₃H₈ than the Pt/Al₂O₃ catalyst (Table 4), indicating that the former was highly active for the oxidation of CO and hydrocarbons. The higher oxidation activities of CO and C₃H₆ on Pd/Al₂O₃ than on Pt/Al₂O₃ is also found in the literature.^{59,60} It should be noted that the dispersion of our catalysts was significantly higher for Pd/Al₂O₃ than for Pt/Al₂O₃, as evidenced by CO chemisorption (Table 1), which resulted in more active sites for the oxidation reactions. Pt/Al₂O₃ had first a rapid increase in the conversion of CO, followed by a small decrease, and then an increase again (Figure 7b, black solid curve, the first cycle). A possible reason for this could be that some of the Pt sites were being oxidized during the first ramp and therefore produced lower activity. The peak in CO conversion in the second ramp experiment was not visible, and in contrast, the conversion of CO was lower in the low-temperature region, indicating the transformation of some Pt sites during the first ramp.

Although Pd/Al₂O₃ initially converted NO at a low temperature, approximately 160 °C, the oxidation of NO was poor up to 350 °C with a planar conversion of less than 10%. The activity then slightly increased and peaked at approximately 450 °C with 21% conversion. NO₂ formation decreased at a higher temperature due to thermodynamical equilibrium limitations.⁶¹ In contrast, for Pt/Al₂O₃ the NO oxidation started at approximately 210 °C, and then quickly peaked at 260 °C with a conversion of 60%. The NO light-off coincided with the C₃H₆ light-off and the reason for this could be that the C₃H₆ species blocked the Pt sites and that C₃H₆ oxidation frees up sites for the NO oxidation reaction.¹² The NO oxidation of this sample decreased at higher temperatures; however, the decrease in NO₂ formation was faster than thermodynamic equilibrium. The decrease in NO conversion seemed to follow a trend similar to the conversion of C₃H₈. It is possible that when the temperature increases, the C₃H₈ is activated resulting in that hydrocarbon species block some Pt sites used for NO oxidation. To verify this hypothesis, we performed additional experiments of gas mixtures with different ratios of NO/C₃H₈ (1:2, 1:1, and 2:1) and in the presence of 500 ppm of C₃H₆ in the mixture of NO/C₃H₈ = 1:1. As shown in Figure S2, the NO conversions at temperatures lower than 200 °C were almost similar; however, the NO conversion significantly decreased with an increase in the concentration of the added C₃H₈ at temperatures higher than 200 °C. Moreover, the presence of C₃H₆ caused a tremendous increase in the light-off temperature of the catalyst for NO oxidation. The oxidation of C₃H₈ on Pt/Al₂O₃ was different from the oxidation on Pd/Al₂O₃; the former had a lower ignition temperature but a slower increase in reaction rate when the temperature increased, resulting in a higher T_{50} of C₃H₈. This result was similar to that reported by Kim and co-workers.⁶⁰ Note that at 450 °C the Pd/Al₂O₃ catalyst had reached full conversion of C₃H₈, while the conversion for the Pt/Al₂O₃ catalyst was only 80% at 500 °C.

Bimetallic Pd–Pt/Al₂O₃, which has about half the amount of Pt and Pd of monometallic catalysts (i.e., the same number of moles of noble metals), had a synergetic effect in its catalytic performance compared to the monometallic counterparts. The Pd–Pt/Al₂O₃ catalyst showed a T_{50} value for C₃H₈ that was similar to the value for Pd/Al₂O₃. The bimetallic catalyst lowered the T_{50} value for the conversion of CO and C₃H₆

compared to Pd/Al₂O₃, even though the Pd–Pt/Al₂O₃ only contained half the amount of Pd. The T_{50} value for CO (164 °C) and C₃H₆ (177 °C) over Pd–Pt/Al₂O₃ was found to be similar to those recently reported for a Pt–Pd/Al₂O₃ catalyst under low-temperature combustion of diesel (LTC-D), for example, T_{50} = 160 and 174 °C for CO and C₃H₆, respectively.⁸ It has also been reported in the literature that a Pd–Pt alloy enhanced the oxidation of CO and C₃H₆,⁶² which is in line with our results. The promotion of CO oxidation occurred because the Pd in a bimetallic alloy improves the amount of CO adsorption in the form of the coadsorbed carbonyl with oxygen (CO–M–O). Subsequently, the available oxygen lowered the light-off temperature.⁶²

The Pd–Pt/Al₂O₃ catalyst not only had a low ignition temperature for NO oxidation, similar to that for Pd/Al₂O₃ but also had a bimodal temperature profile with a maximum of conversion at approximately 260 °C (43%) and 410 °C (35%). The decrease in NO_x conversion around 280 to 350 °C coincides with the propane light-off. We suggest that hydrocarbon species from the propane during light-off might adsorb on the active sites for NO oxidation, in the same way as for the Pt/Al₂O₃, resulting in a decreased NO oxidation (see Figure S2). At higher temperatures when the rate for propane oxidation is higher, more sites are again free for the NO oxidation reaction and the NO₂ formation again increases. NO conversion at 260 °C was 43%, which was lower than the conversion for Pt/Al₂O₃. This was likely due to a lower Pt loading in the bimetallic catalyst. However, a major benefit of the bimetallic catalyst was that NO oxidation started as early as at 175 °C, compared with 225 °C for Pt/Al₂O₃. We suggest the reason for this high NO oxidation activity at a low temperature is that the light-off of C₃H₆ occurred at a low temperature in the bimetallic catalyst. Some of the Pt sites were blocked by C₃H₆ species before propene light-off, hindering NO oxidation,¹² which we also clearly observed in Figure S2. Our results are in line with the study by Gremminger et al., in which bimodal profiles for Pd/Al₂O₃ and Pd–Pt/Al₂O₃ were found, with the highest conversion for Pt/Al₂O₃.⁸ However, the beneficial effect of bimetallic Pd–Pt/Al₂O₃ for NO oxidation was not significant in that study,⁸ in contrast with the results of the present study. One possible reason for this discrepancy could be that different reducing agents were used.

In addition to the NO₂ product attributable to the oxidation of NO, we also observed the formation of N₂O at approximately 180 °C for Pd/Al₂O₃ and Pd–Pt/Al₂O₃, and at approximately 250 °C for Pt/Al₂O₃ (Figure S3). N₂O had likely formed through the reduction of NO caused by the hydrocarbons. Pd–Pt/Al₂O₃ was the most active catalyst with the formation of approximately 36 ppm of N₂O in the second cycle.

3.2.2. NO Oxidation Stability Tests. After the two temperature ramp experiments, the catalyst (Pd/Al₂O₃, Pt/Al₂O₃, and Pd–Pt/Al₂O₃) was pretreated with a reduction and oxidation step and then examined for NO oxidation stability for 10 h (Figure 8). Note that the focus was on the activity for NO oxidation, and therefore a simplified gas mixture was used in these tests (500 ppm of NO, 10 vol % O₂, and 5 vol % H₂O in Ar), without CO and hydrocarbons to exclude their interference since they generally suppress NO oxidation.^{12,63} Pd/Al₂O₃ was almost inactive at 250 °C and converted only 20% of NO at 450 °C, indicating poor activity. The experiment was therefore conducted by increasing the temperature in steps

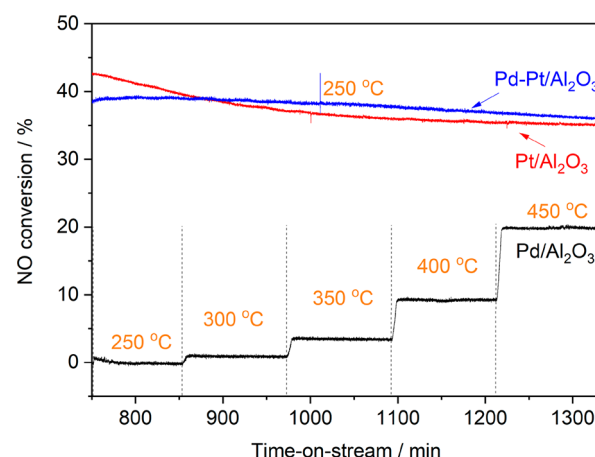


Figure 8. NO conversion on Pd/Al₂O₃, Pt/Al₂O₃, and Pd–Pt/Al₂O₃ catalysts for 10 h; total flow rate of 2600 mL min^{−1} (STP) containing 500 ppm of NO, 10 vol % O₂, and 5 vol % H₂O balanced in Ar. GHSV = 22 520 h^{−1} and temperature at 250 °C for Pt/Al₂O₃ and Pd–Pt/Al₂O₃, and at 250–450 °C (interval of 50 °C, 2 h for each).

from 250 to 450 °C. In contrast, Pt/Al₂O₃ was highly active with an initial NO conversion of 43% at 250 °C. The experiment with Pt/Al₂O₃ was therefore performed for 10 h at the same temperature. However, the conversion of NO on the Pt/Al₂O₃ catalyst slightly deteriorated from 43% to 35% after 10 h of time-on-stream. Interestingly, Pd–Pt/Al₂O₃ was more stable than Pt/Al₂O₃ for NO oxidation; the conversion only decreased from 39% to 36%.

Metallic Pt and PdO are proposed to be the active sites for NO oxidation on monometallic Pt/Al₂O₃ and Pd/Al₂O₃ catalysts, respectively. Metallic Pt was more active than the Pt oxides on the Pt/Al₂O₃ catalyst because metallic Pt has a higher adsorption capacity for NO.^{64–66} PdO was the main active site for NO oxidation on the Pd/Al₂O₃ catalyst as the reaction rate of NO oxidation relies on the mobility of the surface oxygen of PdO clusters.^{67,68} However, NO₂ occupied PdO sites once it had formed and thereby decreased the number of vacancies and limited the mobility of surface oxygen. These factors had an inhibiting effect on NO oxidation.⁶⁷ The NO₂ dissociation with Pt-active sites was easier on the Pt/Al₂O₃ catalyst than the dissociation with O₂, causing high oxygen coverage on these active sites. This blocked the surface of Pt-active sites and decreased NO oxidation activity.⁶⁹ The presence of NO₂ facilitated platinum oxidation, and the platinum oxides that formed had a lower activity for NO oxidation.⁷⁰ The reason for the deterioration in the conversion of NO during the stability tests on the Pt/Al₂O₃ catalyst was likely the formation of Pt oxides caused by the partial oxidation of surface metallic Pt. The addition of Pd to Pt improved the stability of the active sites for NO oxidation. It has been reported that a core–shell formation occurs in bimetallic Pd–Pt, in which the Pt core is protected against oxidation by an exterior shell of Pd, which could explain the more stable activity of the Pd–Pt/Al₂O₃ catalyst than that of the Pt/Al₂O₃ catalyst.⁶⁸ Our XPS results showed that the Pd–Pt/Al₂O₃ catalyst had a more reduced Pt than the Pt/Al₂O₃ catalyst (see Figure 5), which could explain its high stability of NO conversion in Figure 8.

3.2.3. Effect of Pretreatment on Oxidation Activity. The catalyst was activated again with the pretreatment procedure in section 2.4.1 after the NO stability test, and then it was

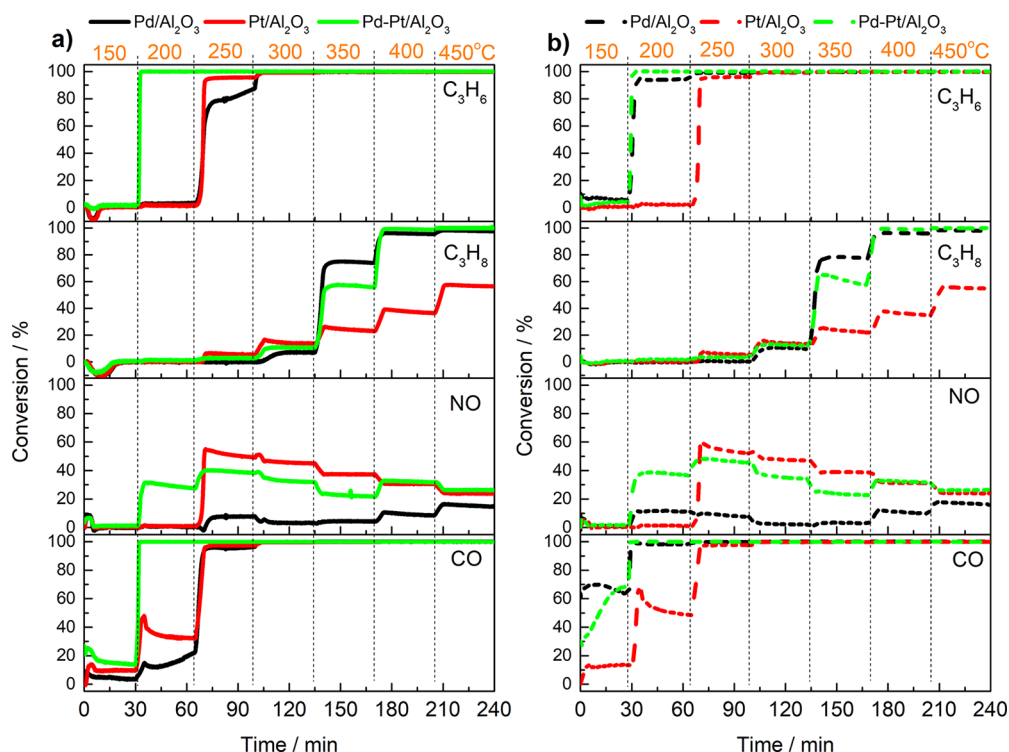


Figure 9. Effect of H_2 pretreatment on conversions of CO, NO, C_3H_8 , and C_3H_6 on $\text{Pd}/\text{Al}_2\text{O}_3$, $\text{Pt}/\text{Al}_2\text{O}_3$, and $\text{Pd-Pt}/\text{Al}_2\text{O}_3$ catalysts at different temperatures: (a) without H_2 pretreatment and (b) with H_2 pretreatment before the activity test; total flow rate of 2600 mL min^{-1} (STP) containing 1000 ppm of CO, 500 ppm of NO, 500 ppm of C_3H_6 , 500 ppm of C_3H_8 , 10 vol % O_2 , and 5 vol % H_2O balanced in Ar. GHSV = 22 520 h^{-1} . Each temperature was maintained for 30 min.

subjected to the activity test at different temperatures from 150 to 450°C (interval of 50°C , so-called T-step) with and without the H_2 pretreatment (Figure 9). All three catalysts functioned well in the oxidation of CO, NO, and C_3H_6 , but not in the oxidation of C_3H_8 . Both CO and C_3H_6 had been completely converted at 300°C , while C_3H_8 had converted less than 20%, with increasing order of $\text{Pd}/\text{Al}_2\text{O}_3$ (7%) < $\text{Pd-Pt}/\text{Al}_2\text{O}_3$ (11%) < $\text{Pt}/\text{Al}_2\text{O}_3$ (14%) (see Figure 9a). The maximum conversion of NO at 250°C was 40 and 50% on the $\text{Pd-Pt}/\text{Al}_2\text{O}_3$ and $\text{Pt}/\text{Al}_2\text{O}_3$ catalysts, respectively. In contrast, the conversion of NO on the $\text{Pd}/\text{Al}_2\text{O}_3$ catalyst was only 8%. Bimetallic $\text{Pd-Pt}/\text{Al}_2\text{O}_3$ had superior oxidation of CO, NO, and C_3H_6 at 200°C . CO and C_3H_6 were completely oxidized, while the conversion of NO was approximately 28%. The monometallic $\text{Pd}/\text{Al}_2\text{O}_3$ and $\text{Pt}/\text{Al}_2\text{O}_3$ catalysts were inactive at 200°C for both C_3H_6 and NO. The conversion of CO was 14 and 33% on the $\text{Pd}/\text{Al}_2\text{O}_3$ and $\text{Pt}/\text{Al}_2\text{O}_3$ catalysts at 200°C , respectively. The superior performance of the bimetallic catalyst at low temperatures can be explained by the presence of abundantly reduced forms of Pt and Pd species in PdO-Pt .

Pretreatment with H_2 significantly improved the oxidation of CO and C_3H_6 on the $\text{Pd}/\text{Al}_2\text{O}_3$ catalyst, but not the oxidation of CO and C_3H_6 on the $\text{Pt}/\text{Al}_2\text{O}_3$ catalyst. The oxidation of hydrocarbons and NO on the $\text{Pt}/\text{Al}_2\text{O}_3$ catalyst was almost unchanged, except for the conversion of CO at 200°C , at which point, the conversion of CO increased from 33 to 48% after the H_2 pretreatment. In contrast, the conversion of CO and C_3H_6 on the $\text{Pd}/\text{Al}_2\text{O}_3$ catalyst largely increased from negligible or low to almost full conversion at 200°C . This catalyst even showed active CO and C_3H_6 oxidation at 150°C . A significant improvement was found for the oxidation of CO on the $\text{Pd-Pt}/\text{Al}_2\text{O}_3$ bimetallic catalyst in which the

conversion of CO increased from 4 to 64% at 150°C after the H_2 pretreatment. These results clearly show that the H_2 pretreatment significantly influenced the oxidation of CO and C_3H_6 on both $\text{Pd}/\text{Al}_2\text{O}_3$ and $\text{Pd-Pt}/\text{Al}_2\text{O}_3$ catalysts but not on the $\text{Pt}/\text{Al}_2\text{O}_3$ catalyst. According to Zorn et al., the palladium oxide on the $\text{Pd}/\text{Al}_2\text{O}_3$ and $\text{Pd-Pt}/\text{Al}_2\text{O}_3$ catalysts can easily be transformed into metallic Pd after the H_2 pretreatment, which is more active than the original PdO form.⁵² In contrast, most of the Pt on the $\text{Pt}/\text{Al}_2\text{O}_3$ catalyst was in metallic form, as evident from XPS data (Figure 5). It is possible that a small fraction of surface platinum oxide could be reduced by H_2 , and this could explain the small increase in CO oxidation at 150°C . This is in line with the XPS results in which a small shift to lower binding energies was observed for the bimetallic catalyst (see Figure 5). The PdO has been reported to be more active for C_3H_8 oxidation than the metallic Pd sites,⁷¹ and subsequently, the H_2 pretreatment might cause a negative effect. However, our data showed that the conversion of C_3H_8 was almost the same after the H_2 pretreatment. Metallic Pd was possibly reoxidized at temperatures higher than 250°C under the lean condition of the gas mixture, which initialized the oxidation of C_3H_8 .

3.2.4. Sulfur Poisoning and Regeneration of DOC. The poisoning and regeneration of sulfur over the monometallic and bimetallic catalysts were investigated. The catalyst was cooled to 200°C in the reaction mixture after the last step (at 450°C) of the T4 test (see Figure 1). The catalyst was stabilized for 30 min at this temperature, and then, 20 ppm of SO_2 was introduced to the reaction mixture (1000 ppm of CO, 500 ppm of NO, 500 ppm of C_3H_6 , 500 ppm of C_3H_8 , 10 vol % O_2 , and 5 vol % H_2O) for 4 h. The SO_2 was then switched off and the reaction was maintained at 200°C for another 30

min. This was followed by cooling the catalyst to 150 °C and a new cycle of T-step tests (T5, 150–450 °C, see Figure 1) was performed. Figure 10 shows the concentration of SO₂ (Figure

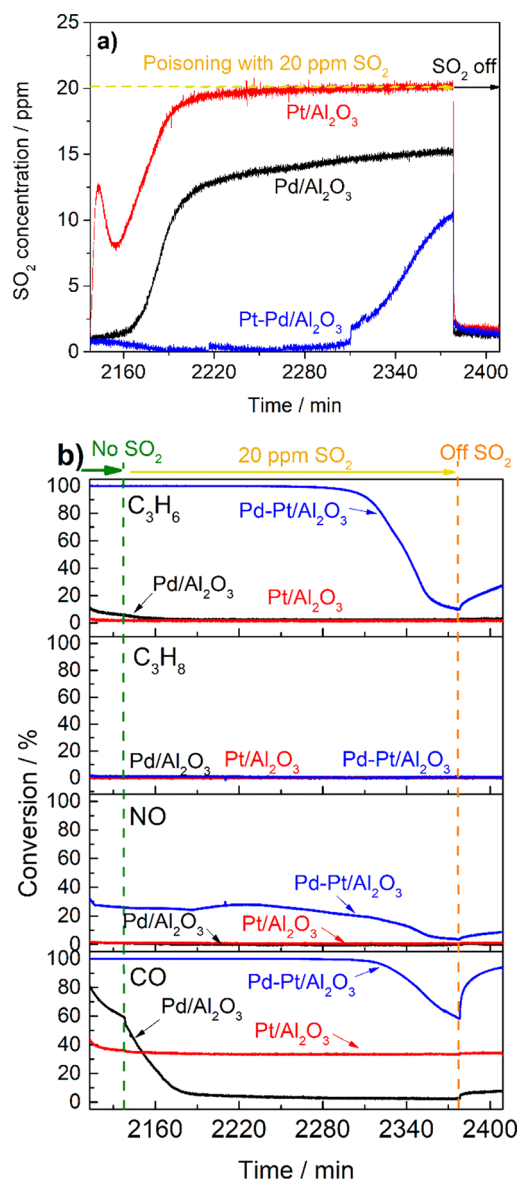


Figure 10. (a) SO₂ concentration profiles and (b) gas conversions (CO, NO, C₃H₈, and C₃H₆) during the sulfur poisoning step at 200 °C for 4 h; total flow rate of 2600 mL min⁻¹ (STP) containing 1000 ppm of CO, 500 ppm of NO, 500 ppm of C₃H₆, 500 ppm of C₃H₈, 10 vol % O₂, and 5 vol % H₂O balanced in Ar. The reaction was performed in a gas mixture at 200 °C for 30 min before 20 ppm of SO₂ was added to the gas mixture for 4 h. Then the reaction was maintained for 30 min more at the same temperature after SO₂ was removed. GHSV = 22 520 h⁻¹.

10a) and the oxidation activity (Figure 10b) over the three catalysts during sulfur poisoning. An immediate breakthrough of SO₂ occurred on the Pt/Al₂O₃ catalyst, whereas the adsorption of SO₂ was extended to approximately 0.5 h on the Pd/Al₂O₃ catalyst. The adsorption of SO₂ onto the Pt/Al₂O₃ catalyst was almost saturated after 1 h of exposure since the SO₂ concentration in the outlet stream almost reached the initial concentration of 20 ppm. However, the adsorption of SO₂ onto the Pd/Al₂O₃ catalyst was not saturated even after 4

h of adsorption (outlet SO₂ concentration approximately 15 ppm at the end of the poisoning). It should be noted that also SO₃ and H₂SO₄ were measured, but the values were in general low and below the level for accurate determination. It was found that the main SO_x source was SO₂. For the Pt/Al₂O₃ catalyst, the SO₂ profile shows lower SO₂ storage initially, which increases and reaches maximum storage after 100 min. Since the gas mixture contains 5 vol % H₂O, the alumina surface is mostly occupied with OH groups. SO₂ can therefore not directly interact with the support but it needs to adsorb on Pt and be oxidized into SO₃, which thereafter can spill over to the support and be captured in the form of sulfates.²¹ Note that before SO₂ was introduced, the catalyst was exposed to the reactants during the cooling and the 30 min reaction at 200 °C before introducing SO₂. It is likely that the Pt species are covered with different HC and NO species and there is a transition time for SO₂ to compete with the Pt sites to get sufficient SO₂ oxidation. We suggest the high initial SO₂ outlet concentration is related to that transition time.

The total adsorption capacity of SO₂ was 0.1 and 0.6 mmol g_{coating}⁻¹ on the Pt/Al₂O₃ and Pd/Al₂O₃ catalysts, respectively. These results show that the Pd/Al₂O₃ catalyst had a higher capacity for the adsorption of SO₂ than the Pt/Al₂O₃ catalyst, which is in line with the results in the literature. Wilburn et al. have found that a Pd–Pt/Al₂O₃ catalyst with a higher content of Pd favored a greater amount of alumina sulfate species.⁷² The bimetallic Pd–Pt/Al₂O₃ catalyst adsorbed SO₂ almost completely up to 170 min, and the catalyst was not saturated by SO₂ even after 4 h of exposure. This resulted in a total capacity for the adsorption of SO₂ of 1.0 mmol g_{coating}⁻¹, which is remarkably higher than that of the monometallic Pd/Al₂O₃ and Pt/Al₂O₃ catalysts.

The impact of SO₂ on the oxidation of each catalyst was evaluated using the conversion of CO, NO, and C₃H₆, but not C₃H₈, because none of the three catalysts was active for C₃H₈ combustion at 200 °C. The conversion of CO on the Pt/Al₂O₃ catalyst was almost constant at 35% during the sulfur-poisoning step, regardless of the addition of 20 ppm of SO₂ (Figure 10b, bottom graph). The Pt/Al₂O₃ catalyst reached saturation of SO₂ quite fast (Figure 10a) indicating that the CO oxidation activity is not maintained by the removal of sulfur species from the Pt by sulfur storage on the support, but instead, is maintained by a high resistance to sulfur poisoning of the Pt sites. In contrast, the conversion of CO on the Pd/Al₂O₃ catalyst dropped immediately as soon as SO₂ was added (Figure 10b, bottom graph), indicating that SO₂ was instantly adsorbed and blocked the PdO-active sites. Complete deactivation occurred after about 1 h of exposure to SO₂, although the adsorption of SO₂ continued for another 3 h, suggesting that SO₂ had been further adsorbed onto the alumina support. The conversion of CO had slightly recovered after SO₂ was removed from the gas mixture. SO₂ did not alter the conversion of CO and C₃H₆ on the bimetallic Pd–Pt/Al₂O₃ catalyst during the first 170 min. It should be noted that the catalyst may have been deactivated during this period, but the conversion of CO and C₃H₆ was so high that no deactivation was visible. The conversion of CO and C₃H₆ had dropped to 59% and 11%, respectively, by the end of the poisoning step. This is in contrast to the Pd/Al₂O₃ catalyst, for which the conversion of CO dropped to zero. These results indicate that SO₂ on the bimetallic Pd–Pt/Al₂O₃ catalyst seemed to adsorb mainly onto the alumina support, evidenced by the large capacity of this catalyst for SO₂ adsorption.

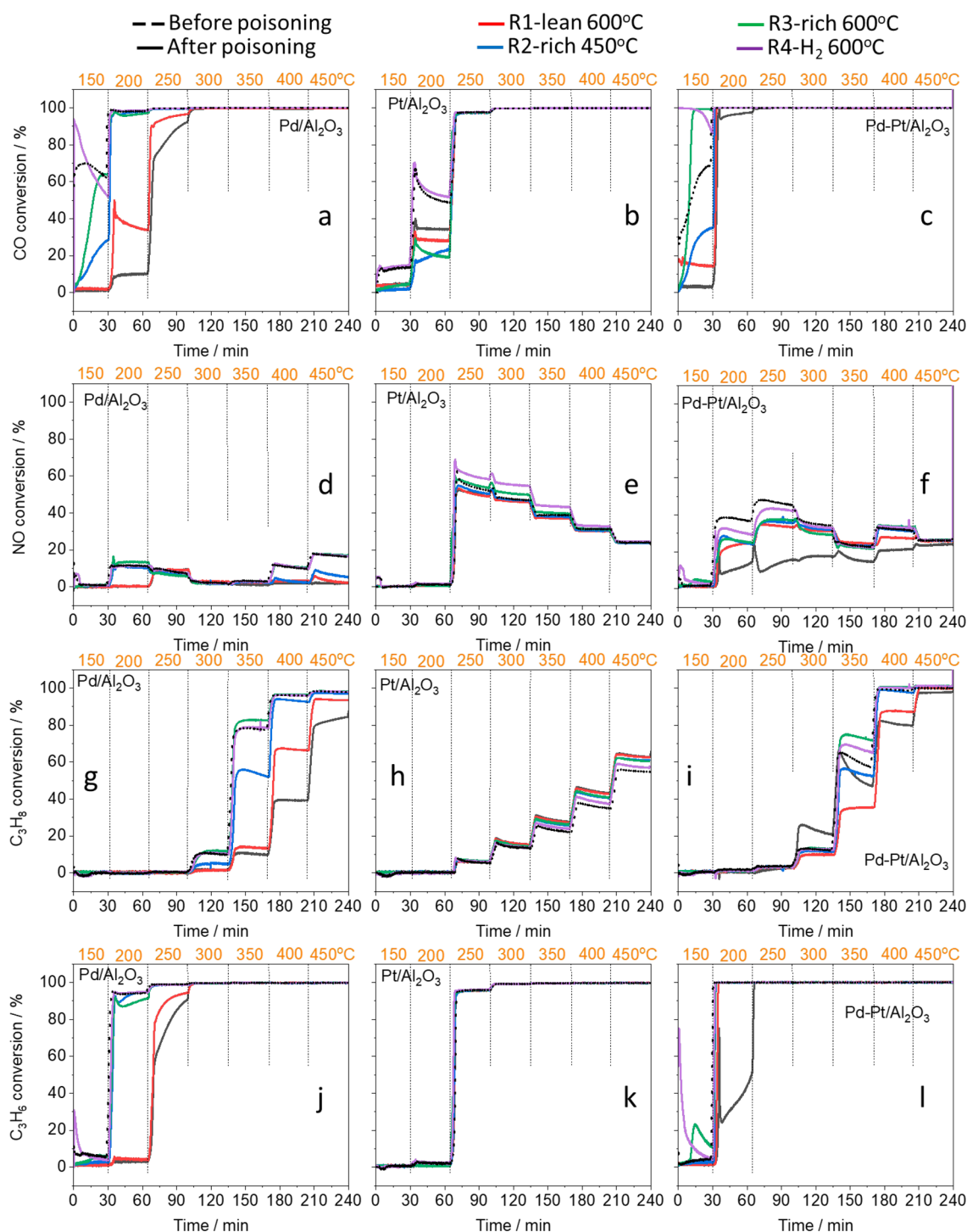


Figure 11. Comparison of conversion profiles of CO, NO, C_3H_8 , and C_3H_6 on Pd/Al_2O_3 , Pt/Al_2O_3 , and $Pd-Pt/Al_2O_3$ catalysts after each regeneration step. Four regeneration steps R1, R2, R3, and R4 were carried out. The conversion of each gas through T-step experiments was compared: before sulfur poisoning (black dotted line), after sulfur poisoning (black solid line), after R1 (red line), after R2 (blue line), after R3 (green line), and after R4 (violet line).

The conversion of C_3H_6 and NO oxidation on the Pd/Al_2O_3 and Pt/Al_2O_3 catalysts was too low prior to the introduction of SO_2 to examine the effect of SO_2 during time-on-stream. The oxidation activity of the bimetallic catalyst partially recovered for C_3H_6 (27%) when SO_2 was switched off, and the activity was close to full conversion for CO (94%) after 30 min. The NO conversion profile on the $Pd-Pt/Al_2O_3$ catalyst showed a general trend like that of C_3H_6 in terms of duration of stability

and deactivation. The conversion of NO on this bimetallic catalyst was somewhat enhanced in the presence of SO_2 after about 1.5–2 h, for instance, the conversion of NO increased from 24.7 to 28.4%. However, the conversion of NO subsequently decreased and was approximately 4.3% at the end of the sulfur poisoning step. The enhancement of SO_2 for NO oxidation could occur because of the low-temperature

sintering effect in the presence of SO₂ on the Pt/Al₂O₃ catalysts, as reported in the literature.^{25,37}

A *T*-step experiment from 150 to 450 °C was carried out after the sulfur poisoning step to determine the impact of SO₂ on the oxidation activity of CO, NO, C₃H₈, and C₃H₆ (denoted “after poisoning”), and then a sequence of four regeneration steps (R1–R4) was performed. The regeneration steps were (i) R1 regeneration with thermal treatment at 600 °C in the gas mixture (lean condition), (ii) R2 and R3 regeneration in rich conditions (switched off O₂ in the gas mixture) at 450 and 600 °C, respectively, and (iv) R4 regeneration in an H₂ environment at 600 °C. A *T*-step experiment from 150 to 450 °C was performed after each regeneration step to evaluate the degree of recovery. The conversion of each gas (CO, NO, C₃H₈, and C₃H₆) in the four *T*-step experiments (after each regeneration step) was then compared with the conversion before and after sulfur poisoning to evaluate the degree of recovery of each catalyst, see Figure 11. Note that the *T*-step experiment directly after the sulfur poisoning could be self-regenerated from 150 to 450 °C before the first regeneration step at 600 °C in the same gas mixture.

Pd/Al₂O₃ catalyst was susceptible to SO₂ poisoning and as a result lost almost all the active sites at low temperature, for example, at 150–200 °C for CO, at 200 °C for NO, at 300–350 °C for C₃H₈, and 200 °C for C₃H₆ (compare the solid and dashed black lines in Figure 11a, d, g, j). The first regeneration step (R1) partially regenerated the activity for CO at 200 °C, C₃H₈ at 400 °C, and C₃H₆ at 250 °C. Additional regeneration steps resulted in the recovery of more active sites at low temperatures, for example, CO at 150 °C, NO at 200 °C, C₃H₈ at 350 °C, and C₃H₆ at 200 °C. The conversion of CO, NO, C₃H₈, and C₃H₆ on the Pd/Al₂O₃ catalyst was fully recovered after the last regeneration step (R4).

The presence of SO₂ was beneficial for C₃H₈ oxidation on Pt/Al₂O₃, in which the conversion of C₃H₈ increased after the sulfur poisoning step. This has also been reported in the literature and explained by the fact that sulfur promotes the dissociative adsorption of C₃H₈ onto Pt,^{31–34} or that it results in the formation of acidic sites at the Pt/Al₂O₃/SO₄^{2–} interface, which enhances the cleavage of the C–C bond of C₃H₈ and, consequently, improves the oxidation of C₃H₈.²⁶ When sulfur regeneration increased, the conversion of propane decreased; however, after R4 the conversion of propane remained higher than before sulfur poisoning, indicating that some sulfur was left. SO₂ did not significantly impact the activity of Pt/Al₂O₃ for NO and C₃H₆ oxidation (Figure 11e, k). However, while all regeneration steps did not alter the activity of C₃H₆ oxidation, the R3 and R4 steps improved the conversion of NO. For example, the conversion of NO at 250 °C was 52% before poisoning (at the end of the temperature step), but the conversion of NO was 58% after the R4 step. We previously observed that sulfur poisoning followed by regeneration can enhance NO oxidation, due to the formation of larger more active Pt particles.²⁵ In contrast, the regeneration steps R1–R3 did not help to recover the activity of CO oxidation at low temperatures; instead, these regeneration steps decreased the conversion of CO. However, the activity had fully recovered after the R4 step (Figure 10b).

Regeneration of the bimetallic Pd–Pt/Al₂O₃ catalyst was more efficient than the regeneration on the Pd/Al₂O₃, for example, the conversion of CO and the oxidation of C₃H₆ had completely recovered after the R1 step at 200 °C. The

conversions were even higher after the R3 and R4 steps than before sulfur poisoning (Figure 11c, l). The improved activity in those steps indicated that a greater number of active sites had been regained after the R3 and R4 steps. Those additional active sites could be metallic Pd species that might have been formed during the reduction of PdO by H₂ during the R4 step, as reported in the literature.⁴⁶ Zorn et al. have reported that metallic Pd or reduced PdO_{*x*} (*x* < 1) was more active for CO oxidation than PdO on alumina support for CO oxidation.⁵² However, the metallic Pd and the reduced PdO_{*x*} (*x* < 1) were reoxidized under lean reaction conditions,⁵² and consequently, the conversion of CO dropped at the end of the step at 150 °C (violet curves in Figure 11a, c). A similar trend was found for CO oxidation on Pd/Al₂O₃ catalyst as well. The conversion of CO after the R4 step was significantly higher in the first 15 min at 150 °C than the conversion of CO before sulfur poisoning. CO and hydrocarbons at 1000 ppm were used in the R3 step and this could result in the formation of metallic Pd under the rich conditions of the step (also during R2). We also observed the formation of CO (see Table S1) during the R3 step. According to Arvajová et al. metallic Pd can be formed through the reduction of PdO_{*x*} with hydrocarbons or CO,⁷³ which agrees well with our results. However, in contrast to the R4 step, the conversion of CO after the R3 step increased with time-on-stream (30 min) at 150 °C (green curves in Figure 11a, c). This suggests that the catalysts had been activated during low temperatures, which was observed for both the Pd/Al₂O₃ and Pd–Pt/Al₂O₃ catalysts. A possible reason for this could be the formation of hydrocarbon species on the noble metal during regeneration in rich conditions, which could be removed in the lean conditions in the *T*-step experiment.

The improvement in C₃H₆ oxidation after the R3 and R4 steps can be explained similarly to the improvement in CO oxidation, which was due to the reduction of PdO to metallic Pd. The positive effect of H₂ pretreatment on Pd-based catalysts for the oxidation of C₃H₆ was also reported in the literature.⁷⁴ The conversion of C₃H₈ increased at 300 °C after the sulfur poisoning step (compare solid and dashed black curves in Figure 11i), but it then decreased at higher temperatures (350 to 450 °C). The conversion of C₃H₆ at 300 °C was completely recovered after all regeneration steps. The activity after the R3 and R4 was even better at 350 °C than before the poisoning step, however, it was slightly lower after the R4 step than after R3. The beneficial effect of SO₂ on propane oxidation has been observed earlier,^{31–34} and the present results suggest that sulfur remained on the surface of the catalysts after regeneration steps, although there was a lower amount of sulfur after the R4 step. About 50% of NO oxidation was regained at 200 °C after the R1 step, similar to the findings after both the R2 and R3 steps (Figure 11f). Although the conversion of NO recovered additionally after the R4 step, it had reached only 75% of its initial oxidation before the poisoning step.

4. CONCLUSIONS

In summary, this work investigated the activity of diesel oxidation catalysts (monometallic Pd/Al₂O₃, Pt/Al₂O₃ and bimetallic Pd–Pt/Al₂O₃ catalysts) focusing on three main aspects: (i) oxidation activity of CO, NO, C₃H₈, and C₃H₆, (ii) NO oxidation stability, (iii) sulfur poisoning and regeneration ability. The bimetallic Pd–Pt/Al₂O₃ possessed an alloy of Pd–Pt and maintained Pd in a reduced phase, in contrast to the monometallic Pd/Al₂O₃ catalyst in which Pd existed in the

oxidized form PdO. The monometallic Pd/Al₂O₃ catalyst had a high conversion for the oxidation of CO and hydrocarbons, whereas the Pt/Al₂O₃ was highly active for NO oxidation. The bimetallic Pd–Pt/Al₂O₃ catalyst showed superior activity compared to its monometallic counterparts due to the synergetic effect of the formation of a Pd–Pt alloy. The bimetallic Pd–Pt/Al₂O₃ exhibited a lower light-off temperature for CO and C₃H₆ oxidation than the Pd/Al₂O₃ catalyst. The conversion of C₃H₈ on the Pd–Pt/Al₂O₃ catalyst was similar to that on the Pd/Al₂O₃ catalyst, although it contained only half of the amount of Pd. In comparison with the Pt/Al₂O₃ catalyst, the Pd–Pt/Al₂O₃ oxidized NO at a lower temperature (around 200 °C) and had greater stability with time-on-stream for NO oxidation. This was likely due to a higher oxidation resistance of Pd–Pt alloy than the monometallic Pt. Exposure to a SO₂-containing gas mixture resulted in stable sulfates on the Pd–Pt/Al₂O₃ catalyst, and thereby a great storage capacity for SO₂. This extensively prolonged the lifetime of the catalyst, but on the other hand made it more difficult to remove sulfur from the catalyst.

■ ASSOCIATED CONTENT

Supporting Information

The Supporting Information is available free of charge at <https://pubs.acs.org/doi/10.1021/acs.iecr.0c05622>.

Comparison of XRD patterns of the Pt/Al₂O₃ and Pd–Pt/Al₂O₃ catalysts after calcination and after degreening; effect of hydrocarbons and CO on the conversion of NO; information on N₂O formation during the NO oxidation on different catalysts; CO concentration during the regeneration of different catalysts under rich conditions (PDF)

■ AUTHOR INFORMATION

Corresponding Author

Louise Olsson – Chemical Engineering, Competence Centre for Catalysis, Chalmers University of Technology, Gothenburg S-412 96, Sweden; orcid.org/0000-0002-8308-0784; Phone: +46 31 772 4390; Email: louise.olsson@chalmers.se

Authors

Phuoc Hoang Ho – Chemical Engineering, Competence Centre for Catalysis, Chalmers University of Technology, Gothenburg S-412 96, Sweden

Jung-Won Woo – Volvo Group Trucks Technology, Gothenburg SE-405-08, Sweden

Rojin Feizie Ilmasani – Chemical Engineering, Competence Centre for Catalysis, Chalmers University of Technology, Gothenburg S-412 96, Sweden

Joonsoo Han – Chemical Engineering, Competence Centre for Catalysis, Chalmers University of Technology, Gothenburg S-412 96, Sweden

Complete contact information is available at: <https://pubs.acs.org/doi/10.1021/acs.iecr.0c05622>

Notes

The authors declare no competing financial interest.

■ ACKNOWLEDGMENTS

We acknowledge the financial support of this FFI project (Grant No. 48038-1) from the Swedish Energy Agency,

Johnson Matthey, and Volvo AB. We would like to thank Dr. Lennart Andersson and Dr. Martin Petersson at Volvo AB and Dr. Gudmund Smedler, Dr. Francois Moreau, and Dr. Andrew Chiffey at Johnson Matthey for valuable discussions. We also acknowledge Dr. Andreas Schaefer and Dr. Anne Wendel at the Division of Applied Chemistry; Dr. Stefan Gustavsson at CMAL; and Dr. Eric Tam at the Department of Industrial and Materials Science (Chalmers University of Technology) for their assistance with the CO chemisorption, N₂ physisorption, TEM, and XPS measurements, respectively.

■ REFERENCES

- (1) Russell, A.; Epling, W. S. Diesel Oxidation Catalysts. *Catal. Rev.: Sci. Eng.* **2011**, 53 (4), 337–423.
- (2) Koebel, M.; Madaia, G.; Elsener, M. Selective catalytic reduction of NO and NO₂ at low temperatures. *Catal. Today* **2002**, 73 (3), 239–247.
- (3) Gieshoff, J.; Schäfer-Sindlinger, A.; Spurk, P. C.; van den Tillaart, J. A. A.; Garr, G. Improved SCR Systems for Heavy Duty Applications. *SAE Tech. Pap. Ser.* **2000**, No. 0189, DOI: 10.4271/2000-01-0189.
- (4) Kallinen, K.; Moreno, A.; Savimäki, A.; Kinnunen, T.-J. J. Pt/Pd Diesel Oxidation Catalyst: A Study on the Properties Enhanced by the Use of Pd. *SAE Tech. Pap. Ser.* **2009**, No. 0018, DOI: 10.4271/2009-26-0018.
- (5) Kim, C. H.; Schmid, M.; Schmieg, S. J.; Tan, J.; Li, W. The Effect of Pt-Pd Ratio on Oxidation Catalysts Under Simulated Diesel Exhaust. *SAE Tech. Pap. Ser.* **2011**, No. 1134, DOI: 10.4271/2011-01-1134.
- (6) Morlang, A.; Neuhausen, U.; Klementiev, K. V.; Schütze, F. W.; Miehe, G.; Fuess, H.; Lox, E. S. Bimetallic Pt/Pd diesel oxidation catalysts: Structural characterisation and catalytic behaviour. *Appl. Catal., B* **2005**, 60 (3), 191–199.
- (7) Shaky, B. M.; Sukumar, B.; López-De Jesús, Y. M.; Markatou, P. The Effect of Pt:Pd Ratio on Heavy-Duty Diesel Oxidation Catalyst Performance: An Experimental and Modeling Study. *SAE Int.* **2015**, 8, 1271.
- (8) Gremminger, A.; Pihl, J.; Casapu, M.; Grunwaldt, J.-D.; Toops, T. J.; Deutschmann, O. PGM based catalysts for exhaust-gas after-treatment under typical diesel, gasoline and gas engine conditions with focus on methane and formaldehyde oxidation. *Appl. Catal., B* **2020**, 265, 118571.
- (9) Martin, N. M.; Nilsson, J.; Skoglundh, M.; Adams, E. C.; Wang, X.; Velin, P.; Smedler, G.; Raj, A.; Thompsett, D.; Brongersma, H. H.; Grehl, T.; Agostini, G.; Mathon, O.; Carlson, S.; Norén, K.; Martinez-Casado, F. J.; Matej, Z.; Balmes, O.; Carlsson, P.-A. Characterization of Surface Structure and Oxidation/Reduction Behavior of Pd–Pt/Al₂O₃ Model Catalysts. *J. Phys. Chem. C* **2016**, 120 (49), 28009–28020.
- (10) Johns, T. R.; Gaudet, J. R.; Peterson, E. J.; Miller, J. T.; Stach, E. A.; Kim, C. H.; Balogh, M. P.; Datye, A. K. Microstructure of Bimetallic Pt-Pd Catalysts under Oxidizing Conditions. *ChemCatChem* **2013**, 5 (9), 2636–2645.
- (11) Kinnunen, N. M.; Hirvi, J. T.; Suvanto, M.; Pakkanen, T. A. Methane combustion activity of Pd–PdO_x–Pt/Al₂O₃ catalyst: The role of platinum promoter. *J. Mol. Catal. A: Chem.* **2012**, 356, 20–28.
- (12) Auvray, X.; Olsson, L. Stability and activity of Pd-, Pt- and Pd–Pt catalysts supported on alumina for NO oxidation. *Appl. Catal., B* **2015**, 168–169, 342–352.
- (13) Sadokhina, N.; Smedler, G.; Nylén, U.; Olofsson, M.; Olsson, L. Deceleration of SO₂ poisoning on PtPd/Al₂O₃ catalyst during complete methane oxidation. *Appl. Catal., B* **2018**, 236, 384–395.
- (14) Lapisardi, G.; Gélín, P.; Kaddouri, A.; Garbowski, E.; Da Costa, S. Pt–Pd bimetallic catalysts for methane emissions abatement. *Top. Catal.* **2007**, 42 (1), 461–464.
- (15) Graham, G. W.; Jen, H. W.; Ezekoye, O.; Kudla, R. J.; Chun, W.; Pan, X. Q.; McCabe, R. W. Effect of alloy composition on

dispersion stability and catalytic activity for NO oxidation over alumina-supported Pt–Pd catalysts. *Catal. Lett.* **2007**, *116* (1), 1–8.

(16) Li, J.; Kumar, A.; Chen, X.; Currier, N.; Yezerets, A. Impact of Different Forms of Sulfur Poisoning on Diesel Oxidation Catalyst Performance. *SAE Tech. Pap. Ser.* **2013**, No. 0514, DOI: 10.4271/2013-01-0514.

(17) Smirnov, M. Y.; Kalinkin, A. V.; Pashis, A. V.; Sorokin, A. M.; Noskov, A. S.; Bukhtiyarov, V. I.; Kharas, K. C.; Rodkin, M. A. Comparative XPS Study of Al_2O_3 and CeO_2 /Sulfation in Reactions with SO_2 , $\text{SO}_2 + \text{O}_2$, $\text{SO}_2 + \text{H}_2\text{O}$, and $\text{SO}_2 + \text{O}_2 + \text{H}_2\text{O}$. *Kinet. Catal.* **2003**, *44* (4), 575–583.

(18) Kröcher, O.; Widmer, M.; Elsener, M.; Rothe, D. Adsorption and Desorption of SO_x on Diesel Oxidation Catalysts. *Ind. Eng. Chem. Res.* **2009**, *48* (22), 9847–9857.

(19) Colussi, S.; Arosio, F.; Montanari, T.; Busca, G.; Groppi, G.; Trovarelli, A. Study of sulfur poisoning on Pd/ Al_2O_3 and Pd/ CeO_2 / Al_2O_3 methane combustion catalysts. *Catal. Today* **2010**, *155* (1), 59–65.

(20) Hamzehlouyan, T.; Sampara, C. S.; Li, J.; Kumar, A.; Epling, W. S. Kinetic study of adsorption and desorption of SO_2 over $\gamma\text{-Al}_2\text{O}_3$ and Pt/ $\gamma\text{-Al}_2\text{O}_3$. *Appl. Catal., B* **2016**, *181*, 587–598.

(21) Wilburn, M. S.; Epling, W. S. Formation and Decomposition of Sulfite and Sulfate Species on Pt/Pd Catalysts: An SO_2 Oxidation and Sulfur Exposure Study. *ACS Catal.* **2019**, *9* (1), 640–648.

(22) Hamzehlouyan, T.; Sampara, C.; Li, J.; Kumar, A.; Epling, W. Sulfur Poisoning of a Pt/ Al_2O_3 Oxidation Catalyst: Understanding of SO_2 , SO_3 and H_2SO_4 Impacts. *Top. Catal.* **2016**, *59* (10–12), 1028–1032.

(23) Gracia, F. J.; Guerrero, S.; Wolf, E. E.; Miller, J. T.; Kropf, A. J. Kinetics, operando FTIR, and controlled atmosphere EXAFS study of the effect of sulfur on Pt-supported catalysts during CO oxidation. *J. Catal.* **2005**, *233* (2), 372–387.

(24) Li, Y.; Shen, M.; Wang, J.; Wan, T.; Wang, J. Influence of sulfation and regeneration on Pt/ Al_2O_3 for NO oxidation. *Catal. Sci. Technol.* **2015**, *5* (3), 1731–1740.

(25) Olsson, L.; Karlsson, H. The beneficial effect of SO_2 on platinum migration and NO oxidation over Pt containing monolith catalysts. *Catal. Today* **2009**, *147*, S290–S294.

(26) Hinz, A.; Skoglundh, M.; Fridell, E.; Andersson, A. An Investigation of the Reaction Mechanism for the Promotion of Propane Oxidation over Pt/ Al_2O_3 by SO_2 . *J. Catal.* **2001**, *201* (2), 247–257.

(27) Lott, P.; Eck, M.; Doronkin, D. E.; Zimina, A.; Tischer, S.; Popescu, R.; Belin, S.; Briois, V.; Casapu, M.; Grunwaldt, J.-D.; Deutschmann, O. Understanding sulfur poisoning of bimetallic Pd–Pt methane oxidation catalysts and their regeneration. *Appl. Catal., B* **2020**, *278*, 119244.

(28) Wilburn, M. S.; Epling, W. S. Sulfur deactivation and regeneration of mono- and bimetallic Pd–Pt methane oxidation catalysts. *Appl. Catal., B* **2017**, *206*, 589–598.

(29) Meeyoo, V.; Trimm, D. L.; Cant, N. W. The effect of sulphur containing pollutants on the oxidation activity of precious metals used in vehicle exhaust catalysts. *Appl. Catal., B* **1998**, *16* (2), L101–L104.

(30) Mowery, D. L.; McCormick, R. L. Deactivation of alumina supported and unsupported PdO methane oxidation catalyst: the effect of water on sulfate poisoning. *Appl. Catal., B* **2001**, *34* (4), 287–297.

(31) Yao, H. C.; Stepien, H. K.; Gandhi, H. S. The effects of SO_2 on the oxidation of hydrocarbons and carbon monoxide over Pt/ $\gamma\text{-Al}_2\text{O}_3$ catalysts. *J. Catal.* **1981**, *67* (1), 231–236.

(32) Corro, G.; Montiel, R.; Vázquez, L. C. Promoting and inhibiting effect of SO_2 on propane oxidation over Pt/ Al_2O_3 . *Catal. Commun.* **2002**, *3* (11), 533–539.

(33) Lee, A. F.; Wilson, K.; Lambert, R. M.; Hubbard, C. P.; Hurley, R. G.; McCabe, R. W.; Gandhi, H. S. The Origin of SO_2 Promotion of Propane Oxidation over Pt/ Al_2O_3 Catalysts. *J. Catal.* **1999**, *184* (2), 491–498.

(34) Skoglundh, M.; Ljungqvist, A.; Petersson, M.; Fridell, E.; Cruise, N.; Augustsson, O.; Jobson, E. SO_2 promoted oxidation of

ethyl acetate, ethanol and propane. *Appl. Catal., B* **2001**, *30* (3), 315–328.

(35) Wan, J.; Ran, R.; Li, M.; Wu, X.; Weng, D. Effect of acid and base modification on the catalytic activity of Pt/ Al_2O_3 for propene oxidation. *J. Mol. Catal. A: Chem.* **2014**, *383–384*, 194–202.

(36) Kolli, T.; Kanerva, T.; Huuhtanen, M.; Vippola, M.; Kallinen, K.; Kinnunen, T.; Lepistö, T.; Lahtinen, J.; Keiski, R. L. The activity of Pt/ Al_2O_3 diesel oxidation catalyst after sulphur and calcium treatments. *Catal. Today* **2010**, *154* (3), 303–307.

(37) Auvray, X. P.; Olsson, L. Sulfur Dioxide Exposure: A Way To Improve the Oxidation Catalyst Performance. *Ind. Eng. Chem. Res.* **2013**, *52* (41), 14556–14566.

(38) Cabello Galisteo, F.; Mariscal, R.; López Granados, M.; Zafra Poves, M. D.; Fierro, J. L. G.; Kröger, V.; Keiski, R. L. Reactivation of sulphated Pt/ Al_2O_3 catalysts by reductive treatment in the simultaneous oxidation of CO and C_3H_6 . *Appl. Catal., B* **2007**, *72* (3), 272–281.

(39) Bergeret, G.; Gallezot, P. Particle Size and Dispersion Measurements. In *Handbook of Heterogeneous Catalysis*, 2nd ed.; Ertl, G.; Knözinger, H.; Schüth, F.; Weitkamp, J., Eds.; Wiley: Weinheim, 2008; Vol. 2, pp 738–765.

(40) Canton, P.; Fagherazzi, G.; Battagliarin, M.; Menegazzo, F.; Pinna, F.; Pernicone, N. Pd/CO Average Chemisorption Stoichiometry in Highly Dispersed Supported Pd/ $\gamma\text{-Al}_2\text{O}_3$ Catalysts. *Langmuir* **2002**, *18* (17), 6530–6535.

(41) Allian, A. D.; Takanabe, K.; Fujdala, K. L.; Hao, X.; Truex, T. J.; Cai, J.; Buda, C.; Neurock, M.; Iglesia, E. Chemisorption of CO and Mechanism of CO Oxidation on Supported Platinum Nanoclusters. *J. Am. Chem. Soc.* **2011**, *133* (12), 4498–4517.

(42) Narui, K.; Yata, H.; Furuta, K.; Nishida, A.; Kohtoku, Y.; Matsuzaki, T. Effects of addition of Pt to PdO/ Al_2O_3 catalyst on catalytic activity for methane combustion and TEM observations of supported particles. *Appl. Catal., A* **1999**, *179* (1), 165–173.

(43) Nilsson, J.; Carlsson, P.-A.; Martin, N. M.; Adams, E. C.; Agostini, G.; Grönbeck, H.; Skoglundh, M. Methane oxidation over Pd/ Al_2O_3 under rich/lean cycling followed by operando XAFS and modulation excitation spectroscopy. *J. Catal.* **2017**, *356*, 237–245.

(44) Castellazzi, P.; Groppi, G.; Forzatti, P.; Baylet, A.; Marécot, P.; Duprez, D. Role of Pd loading and dispersion on redox behaviour and CH_4 combustion activity of Al_2O_3 supported catalysts. *Catal. Today* **2010**, *155* (1), 18–26.

(45) Moulder, J. F.; Chastain, J. *Handbook of X-ray Photoelectron Spectroscopy: A Reference Book of Standard Spectra for Identification and Interpretation of XPS Data*. Physical Electronics Division, Perkin-Elmer Corporation: MN, 1992; p 153.

(46) Baylet, A.; Marécot, P.; Duprez, D.; Castellazzi, P.; Groppi, G.; Forzatti, P. In situ Raman and in situ XRD analysis of PdO reduction and Pd⁰ oxidation supported on $\gamma\text{-Al}_2\text{O}_3$ catalyst under different atmospheres. *Phys. Chem. Chem. Phys.* **2011**, *13* (10), 4607–4613.

(47) Yudanov, I. V.; Sahnoun, R.; Neyman, K. M.; Rösch, N.; Hoffmann, J.; Schauerhmann, S.; Johánek, V.; Unterhalt, H.; Rupprechter, G.; Libuda, J.; Freund, H.-J. CO Adsorption on Pd Nanoparticles: Density Functional and Vibrational Spectroscopy Studies. *J. Phys. Chem. B* **2003**, *107* (1), 255–264.

(48) Dann, E. K.; Gibson, E. K.; Catlow, R. A.; Collier, P.; Erlep Erden, T.; Gianolio, D.; Hardacre, C.; Kroner, A.; Raj, A.; Goguet, A.; Wells, P. P. Combined In Situ XAFS/DRIFTS Studies of the Evolution of Nanoparticle Structures from Molecular Precursors. *Chem. Mater.* **2017**, *29* (17), 7515–7523.

(49) Zheng, Y.; Kovarik, L.; Engelhard, M. H.; Wang, Y.; Wang, Y.; Gao, F.; Szanyi, J. Low-Temperature Pd/Zelite Passive NO_x Adsorbers: Structure, Performance, and Adsorption Chemistry. *J. Phys. Chem. C* **2017**, *121* (29), 15793–15803.

(50) Knözinger, H.; Huber, S. IR spectroscopy of small and weakly interacting molecular probes for acidic and basic zeolites. *J. Chem. Soc., Faraday Trans.* **1998**, *94* (15), 2047–2059.

(51) Wang, X.; Shi, H.; Kwak, J. H.; Szanyi, J. Mechanism of CO_2 Hydrogenation on Pd/ Al_2O_3 Catalysts: Kinetics and Transient DRIFTS-MS Studies. *ACS Catal.* **2015**, *5* (11), 6337–6349.

- (52) Zorn, K.; Giorgio, S.; Halwax, E.; Henry, C. R.; Grönbeck, H.; Rupprechter, G. CO Oxidation on Technological Pd-Al₂O₃ Catalysts: Oxidation State and Activity. *J. Phys. Chem. C* **2011**, *115* (4), 1103–1111.
- (53) Zhang, Y.; Cai, Y.; Guo, Y.; Wang, H.; Wang, L.; Lou, Y.; Guo, Y.; Lu, G.; Wang, Y. The effects of the Pd chemical state on the activity of Pd/Al₂O₃ catalysts in CO oxidation. *Catal. Sci. Technol.* **2014**, *4* (11), 3973–3980.
- (54) Zhang, Z.; Zhu, Y.; Asakura, H.; Zhang, B.; Zhang, J.; Zhou, M.; Han, Y.; Tanaka, T.; Wang, A.; Zhang, T.; Yan, N. Thermally stable single atom Pt/m-Al₂O₃ for selective hydrogenation and CO oxidation. *Nat. Commun.* **2017**, *8* (1), 16100.
- (55) Bourane, A.; Bianchi, D. Heats of adsorption of the linear CO species on Pt/Al₂O₃ using infrared spectroscopy: impact of the Pt dispersion. *J. Catal.* **2003**, *218* (2), 447–452.
- (56) Benvenutti, E. V.; Franken, L.; Moro, C. C.; Davanzo, C. U. FTIR Study of Hydrogen and Carbon Monoxide Adsorption on Pt/TiO₂, Pt/ZrO₂, and Pt/Al₂O₃. *Langmuir* **1999**, *15* (23), 8140–8146.
- (57) Stakheev, A. Y.; Shpiro, E. S.; Tkachenko, O. P.; Jaeger, N. I.; Schulz-Ekloff, G. Evidence for Monatomic Platinum Species in H-ZSM-5 from FTIR Spectroscopy of Chemisorbed CO. *J. Catal.* **1997**, *169* (1), 382–388.
- (58) Xiong, H.; Peterson, E.; Qi, G.; Datye, A. K. Trapping mobile Pt species by PdO in diesel oxidation catalysts: Smaller is better. *Catal. Today* **2016**, *272*, 80–86.
- (59) Ivanova, A. S.; Slavinskaya, E. M.; Gulyaev, R. V.; Zaikovskii, V. I.; Stonkus, O. A.; Danilova, I. G.; Plyasova, L. M.; Polukhina, I. A.; Boronin, A. I. Metal-support interactions in Pt/Al₂O₃ and Pd/Al₂O₃ catalysts for CO oxidation. *Appl. Catal., B* **2010**, *97* (1), 57–71.
- (60) Kim, J.; Kim, Y.; Wiebenga, M. H.; Oh, S. H.; Kim, D. H. Oxidation of C₃H₈, iso-C₅H₁₂ and C₃H₆ under near-stoichiometric and fuel-lean conditions over aged Pt–Pd/Al₂O₃ catalysts with different Pt:Pd ratios. *Appl. Catal., B* **2019**, *251*, 283–294.
- (61) Olsson, L.; Westerberg, B.; Persson, H.; Fridell, E.; Skoglundh, M.; Andersson, B. A kinetic study of oxygen adsorption/desorption and NO oxidation over Pt/Al₂O₃ catalysts. *J. Phys. Chem. B* **1999**, *103* (47), 10433–10439.
- (62) Hazlett, M. J.; Moses-Debusk, M.; Parks, J. E.; Allard, L. F.; Epling, W. S. Kinetic and mechanistic study of bimetallic Pt–Pd/Al₂O₃ catalysts for CO and C₃H₆ oxidation. *Appl. Catal., B* **2017**, *202*, 404–417.
- (63) Irani, K.; Epling, W. S.; Blint, R. Effect of hydrocarbon species on NO oxidation over diesel oxidation catalysts. *Appl. Catal., B* **2009**, *92* (3), 422–428.
- (64) Bhatia, D.; McCabe, R. W.; Harold, M. P.; Balakotaiah, V. Experimental and kinetic study of NO oxidation on model Pt catalysts. *J. Catal.* **2009**, *266* (1), 106–119.
- (65) Benard, S.; Retailleau, L.; Gaillard, F.; Vernoux, P.; Giroir-Fendler, A. Supported platinum catalysts for nitrogen oxide sensors. *Appl. Catal., B* **2005**, *55* (1), 11–21.
- (66) Weiss, B. M.; Iglesia, E. NO Oxidation Catalysis on Pt Clusters: Elementary Steps, Structural Requirements, and Synergistic Effects of NO₂ Adsorption Sites. *J. Phys. Chem. C* **2009**, *113* (30), 13331–13340.
- (67) Weiss, B. M.; Iglesia, E. Mechanism and site requirements for NO oxidation on Pd catalysts. *J. Catal.* **2010**, *272* (1), 74–81.
- (68) Kaneeda, M.; Iizuka, H.; Hiratsuka, T.; Shinotsuka, N.; Arai, M. Improvement of thermal stability of NO oxidation Pt/Al₂O₃ catalyst by addition of Pd. *Appl. Catal., B* **2009**, *90* (3), 564–569.
- (69) Getman, R. B.; Schneider, W. F.; Smeltz, A. D.; Delgass, W. N.; Ribeiro, F. H. Oxygen-Coverage Effects on Molecular Dissociations at a Pt Metal Surface. *Phys. Rev. Lett.* **2009**, *102* (7), 076101.
- (70) Olsson, L.; Fridell, E. The influence of Pt oxide formation and Pt dispersion on the reactions NO₂ ⇌ NO + 1/2 O₂ over Pt/Al₂O₃ and Pt/BaO/Al₂O₃. *J. Catal.* **2002**, *210* (2), 340–353.
- (71) Khudorozhkov, A. K.; Chetyrin, I. A.; Bukhtiyarov, A. V.; Prosvirin, I. P.; Bukhtiyarov, V. I. Propane Oxidation Over Pd/Al₂O₃: Kinetic and In Situ XPS Study. *Top. Catal.* **2017**, *60* (1), 190–197.
- (72) Wilburn, M. S.; Epling, W. S. SO₂ adsorption and desorption characteristics of bimetallic Pd–Pt catalysts: Pd:Pt ratio dependency. *Catal. Today* **2019**, *320*, 11–19.
- (73) BuzkováÁrvajová, A.; Boutikos, P.; Pečinka, R.; Kočí, P. Global kinetic model of NO oxidation on Pd/γ-Al₂O₃ catalyst including PdO_x formation and reduction by CO and C₃H₆. *Appl. Catal., B* **2020**, *260*, 118141.
- (74) Aznárez, A.; Gil, A.; Korili, S. A. Performance of palladium and platinum supported on alumina pillared clays in the catalytic combustion of propene. *RSC Adv.* **2015**, *5* (100), 82296–82309.